Tbx4 function during hindlimb development reveals a novel mechanism to explain the origins of proximal limb defects

Veronique Duboc[*,3], Fatima Sulaiman, Eleanor Feneck, Anna Kucharska[4], Donald Bell[1], Muriel Holder-Espinasse[2] Malcolm P.O. Logan*.

Randall Centre for Cell and Molecular Biophysics, King's College London, Guy's Campus, London SE1 1UL, UK. [1]Light Microscopy, Francis Crick Institute, 1 Midland Road, London, NW1 1AT, UK. [2]Clinical Genetics Department, Guy's Hospital, London SE1 9RT, UK

Current addresses: [3] Université Côte d'Azur, CHU de Nice, Inserm, CNRS, IRCAN, Nice, France, [4]Stem Cell Biology and Developmental Genetics, Francis Crick Institute, 1 Midland Road, London, NW1 1AT, UK

*Authors for correspondence: malcolm.logan@kcl.ac.uk, duboc.v@chu-nice.fr

Keywords: Congenital limb abnormalities, Chondrogenesis, limb formation, *Tbx4*, *Pitx1*

Summary Statement

This study provides a molecular and cellular mechanism to the causes of proximally-biased limb defects, which can explain the origins of the congenital limb abnormality, phocomelia.

Abstract

We dissect genetically a gene regulatory network, including the transcription factors *Tbx4*, *Pitx1* and *Isl1* that act cooperatively to establish the hindlimb bud and identify key differences in the pathways that initiate formation of the hindlimb and forelimb. Using live image analysis of limb mesenchyme cells undergoing chondrogenesis in micromass culture,

we distinguish a series of changes in cellular behaviours and cohesiveness that are required for chondrogenic precursors to undergo differentiation. Furthermore, we provide evidence that the proximal hindlimb defects in the *Tbx4* mutant result from a failure in the early differentiation step of chondroprogenitors into chondrocytes, providing a novel explanation for the origins of proximally-biased limb defects.

Introduction

Forelimbs and hindlimbs arise as outgrowths from the lateral plate mesoderm and form at fixed positions along the body axis. Forelimbs form at the cervical/thoracic junction while hindlimbs form at the lumbar/sacral junction and this position is conserved in vertebrates even when the number of segments/vertebrae differs between different species (Burke et al. 1995, Nishimoto and Logan 2016). Initiation of forelimb and hindlimb formation starts with either the expression of the T-box transcription factors, *Tbx5* or *Tbx4*, in restricted regions of the future forelimb- and hindlimb-forming lateral plate mesoderm, respectively. A key function of *Tbx5* and *Tbx4* is to activate *Fgf10* expression and establish an FGF-signalling, positive feedback loop that drives limb bud outgrowth (Nishimoto and Logan 2016). This feedback loop is required for limb bud outgrowth and *Fgf10* mutant mice lack both forelimbs and hindlimbs (Sekine et al. 1999). Therefore, despite *Tbx4* and its paralogue *Tbx5* having dramatic hindlimb- and forelimb-restricted expression patterns, respectively (Logan et al. 1998, Rallis et al. 2003) both appear to have common roles in establishing limb bud formation by activating and establishing expression of *Fgf10* (Minguillon et al. 2005, Nishimoto and Logan 2016, Nishimoto et al. 2015).

There are important differences, however, in how the forelimb and hindlimb buds are established. In the forelimb, *Tbx5* input is essential for *Fgf10* expression, while in the *Tbx4* mutant hindlimb some *Fgf10* expression is initiated and a small hindlimb bud forms (Naiche and Papaioannou 2003). Therefore, although *Tbx4* is necessary for normal hindlimb *Fgf10* expression there is not the same exclusive requirement for *Tbx4* activity in the hindlimb to establish *Fgf10* expression as there is for its paralogue, *Tbx5*, in the forelimb. Additional inputs from other genes, such as *Islet1* (*Isl1*) appear to be required for the establishment of normal *Fgf10* expression in the hindlimb (Itou et al. 2012, Kawakami et al. 2011, Narkis et al. 2012).

To explore the differences in the pathways that establish the hindlimb bud, we have generated a complete loss of function of *Tbx4* in the hindlimb using a cre-deleter line, *RetRV5Cre*, which drives expression of cre recombinase throughout the hindlimb bud mesenchyme prior to hindlimb bud initiation. We demonstrate that there are significant differences between the forelimb and hindlimb initiation processes. Unlike in the forelimb, a dual input from *Tbx4* and the paired homeodomain transcription factor, *Pitx1*, are necessary to initiate *Fgf10* expression and drive further growth of the hindlimb bud. Furthermore, we clarify the epistatic relationship between *Tbx4*, *Pitx1* and *Isl1* during hindlimb budding, by showing that *Isl1* acts in parallel to *Pitx1* and *Tbx4* to initiate *Fgf10* expression. This distinction between forelimb and hindlimb developmental processes reveals an unexpected role for *Tbx4* during the formation of proximal skeletal elements.

We further demonstrate, using a gene deletion-gene replacement strategy, that in the absence of *Tbx4* expression, *Tbx5* can fully rescue hindlimb formation, further demonstrating that both paralogous genes exert identical function during the development of forelimb and hindlimb. Furthermore, using an inducible *Fgf10* transgenic, *Z/EGFgf10*, we show that the proximal bias of the phenotype observed in the *Tbx4* conditional mutant cannot solely be explained by the reduction of Fgf10 ligand expression. Finally, we provide evidence that the proximal hindlimb defects in the *Tbx4* mutant do not arise as a consequence of incorrect proximo-distal patterning, absence of *Fgf8* expression or cell death, but from a failure in the early differentiation step of chondroprogenitors into chondrocytes.

Results

Conditional deletion of *Tbx4* produces proximally-biased hindlimb defects

The function of *Tbx4* in the hindlimb has been assessed previously by conditional deletion, using a constitutively active Cre and the limb-restricted *Prrx1Cre* transgene (Naiche and Papaioannou 2003, 2007). Interpretation of the role of *Tbx4* in hindlimb initiation has proven difficult, however, since broad deletion of *Tbx4* is embryonic lethal at early limb bud stages and the *Prrx1Cre* transgene is active in the hindlimb bud only after it has formed (Logan et al. 2002). Following constitutive deletion of *Tbx4*, *Fgf10* expression in the nascent hindlimb-forming region is reduced and a small hindlimb bud forms (Naiche and Papaioannou 2003). This is in marked contrast to the forelimb where conditional deletion of *Tbx5* leads to a failure to establish *Fgf10* expression and, as a consequence, complete absence of the forelimb bud. To conditionally delete *Tbx4* in the hindlimb-forming region, we generated a cre deleter transgenic mouse using a regulatory element from the *Ret* gene (Sukumaran et al. 2001). The activity of this isolated regulatory fragment does not replicate endogenous *Ret* expression from the intact locus. The *RetRVCre* line produces robust cre activity in the hindlimb forming

region prior to hindlimb bud formation (Supplementary Fig.1) and, significantly, this restricted expression does not generate the chorio-allantoic fusion defects observed in the constitutive *Tbx4* mutant (Naiche and Papaioannou 2003). The *RetRVCre* deleter is therefore able to effectively conditionally delete *Tbx4* in the cells that normally give rise to the hindlimb without producing an early embryonic lethal phenotype (see below). We produced *Tbx4* mutant embryos that were either homozygous for the *Tbx4* conditional allele (*Tbx4*$^{lox/lox}$*;RetRVCre*) (Fig.1C) or carried one conditional allele and one deleted allele (*Tbx4*$^{\Delta/lox}$*;RetRVCre*) (Fig.1D). In both cases mutant embryos at E17.5 form a small, rudimentary hindlimb comprising a tibia, a few malformed metatarsal and tarsal elements and 2-4 digits in the distal extreme. The morphology of the most anterior digit most closely resembles digit 1, therefore we propose a loss of an intermediate digit(s). In control embryos, the pelvis anchors the hindlimb to the spine. Strikingly, in mutant embryos, the most proximal elements, the femur and pelvis, are either absent or severely hypoplastic (Fig.1C,D,F). The most proximal elements that do form (tibia) lack any connection with the main body axis (Fig.1C,D,F).

Dual inputs from *Tbx4* and *Pitx1* are required for hindlimb initiation

At E10.5, *Tbx4*$^{lox/lox}$*;RetRVCre* hindlimbs buds are smaller than controls and expression of *Fgf10* is reduced, although detectable (Supplementary Fig.2 A,B) demonstrating that, in the absence of *Tbx4*, another factor can partially compensate to regulate *Fgf10* expression. This is in contrast to the forelimb where there is an exclusive requirement for *Tbx5* for initiation of *Fgf10* expression (Rallis et al. 2003). *Pitx1* is a candidate factor to act in addition to *Tbx4* in regulating *Fgf10*. *Pitx1*$^{-/-}$ mutant mice form a small hindlimb that has lost some of its characteristic hindlimb morphologies such as the presence of a patella (Duboc and Logan 2011a, b, Marcil et al. 2003, Szeto et al. 1999) and (Fig.1G)). *Pitx1* is known to be partially

required for normal levels of *Tbx4* expression (Duboc and Logan 2011b, Marcil et al. 2003, Szeto et al. 1999) whereas *Pitx1* expression is unaffected following conditional deletion of *Tbx4* (Supplementary Fig.2D-E). We therefore generated *Tbx4*/*Pitx1* compound mutants (*Pitx1*$^{-/-}$;*Tbx4*$^{lox/lox}$;*RetRVCre*) and in these compound mutants no hindlimb elements are present (Fig.1H). Moreover, *Fgf10* expression is not detectable in the hindlimb-forming region at hindlimb budding stages (Supplementary Fig.2C). These results demonstrate that *Pitx1* and *Tbx4* have dual inputs that are required for *Fgf10* expression and subsequent hindlimb formation.

Islet1 acts in parallel to *Tbx4* and *Pitx1* during hindlimb initiation

A third factor, that has been implicated in the initiation of hindlimb outgrowth specifically, is the LIM homeodomain transcription factor *Islet1* (*Isl1*) (Itou et al. 2012, Kawakami et al. 2011, Narkis et al. 2012). *Isl1* and its obligatory co-regulators *Ldb1/Ldb2* are essential for hindlimb formation through their regulation of *Fgf10* but they are not required for *Tbx4* or *Pitx1* expression (Kawakami et al. 2011, Narkis et al. 2012). *Isl1* expression is unaffected in either the *Pitx1* mutant (*Pitx1*$^{-/-}$), *Tbx4* conditional mutant (*Tbx4*$^{lox/lox}$;*RetRVCre*) or *Pitx1/Tbx4* compound mutant (*Pitx1*$^{-/-}$;*Tbx4*$^{lox/lox}$;*RetRVCre*) (Fig.2C-H) at hindlimb initiation stage (E10.0) demonstrating that *Tbx4* and *Pitx1* are not required for *Isl1* expression. Therefore, since *Isl1*/*Ldb1/2* do not act upstream or downstream of *Tbx4* and *Pitx1*, we favour a model in which Isl1/Ldb1/2 act as obligate cofactors with Tbx4 and Pitx1, functioning in parallel to regulate *Fgf10* expression (Fig.3A).

Tbx5 but not _Fgf10_ can rescue hindlimb proximal defects in the absence of _Tbx4_

Fgf10 is essential for limb bud formation and it is a target of _Tbx4/5_. To determine whether direct regulation of _Fgf10_ expression is the primary function of _Tbx4/5_ during the initial phase of limb bud formation, we compared the abilities of _Tbx4_ and _Tbx5_ and their downstream target, _Fgf10_, to rescue hindlimb formation in the _Tbx4_ conditional mutant using a gene deletion/gene replacement strategy. As a control experiment, we crossed transgenic lines expressing either _Tbx4_ or _Tbx5_ under control of the _Prrx1_ regulatory element (_Prrx1-Tbx4_; _Prrx1-Tbx5_; (Duboc and Logan 2011b, Minguillon et al. 2005) into the background of the _Tbx4_ conditional knockout (_Tbx4$^{lox/lox}$;RetRVCre;Prrx1-Tbx4_ and _Tbx4$^{lox/lox}$;RetRVCre;Prrx1-Tbx5_). Both _Tbx4_ and _Tbx5_ transgenes are able to rescue hindlimb development in the _Tbx4_ conditional knockout background (Fig.3D,F). Consistent with our previous observations (Duboc and Logan 2011b, Minguillon et al. 2005, Minguillon et al. 2009), the _Tbx5_-rescued limb retains all hindlimb characteristics indicating that _Tbx5_ and _Tbx4_ can act equivalently to regulate limb outgrowth and have no role in determining forelimb or hindlimb morphologies in mouse. Using the same strategy with a cre-inducible _Fgf10_ transgenic (_Z/EGFgf10_ see Materials and Methods, (Sulaiman et al. 2016)) produced no discernible rescue of the _Tbx4_ conditional knockout phenotype (Fig.3E). This is despite the fact that the same _Fgf10_-inducible line and cre transgenic are able to fully rescue hindlimb formation in the _Fgf10_ mutant (_Fgf10$^{-/-}$;RetRvCre;Z/EGFgf10_) (Supplementary Fig.3). These results demonstrate that the level of FGF signalling in the hindlimb is not established solely through the direct regulation of Fgf10 ligand by _Tbx4_ and that other _Tbx4_ targets have critical roles in establishing FGF signalling levels sufficient for normal limb outgrowth. In the forelimb, _Tbx5_ acts in a feed-forward loop to regulate both Fgf10 ligand and mesenchymal expression of an FGF receptor that is required to establish the positive

feedback loop of FGF signalling (Harvey and Logan 2006). Our results are consistent with an equivalent relationship existing in the hindlimb (Fig.3A).

Hindlimb proximal defects in the *Tbx4* mutant cannot be explained by defects in proximal-distal specification, absence of *Fgf8* expression or cell death

The limb skeleton is divided into three anatomical segments from proximal to distal: the stylopod (humerus/femur), zeugopod (radius/tibia and ulna/fibula), and autopod (wrist/ankle and digits) (Fig.1A) and the genes, *Meis1/2*, *HoxA11*, and *HoxA13*, respectively, are markers of these territories (Galloway et al. 2009, Rosello-Diez et al. 2011) and (Fig. 4A,C,E). Although the *Tbx4* mutant hindlimbs are smaller, three distinct stylopod, zeugopod and autopod domains are clearly distinguished with these three markers at E10.5 (Supplementary Fig.4A-F) and E11.5 (Fig.4B,D,F) demonstrating that proximal-distal specification can occur in the absence of *Tbx4* and that proximally-biased defects generated in these mutants cannot be explained by failure to establish proximal-distal pattern.

The short stature homeobox gene, *Shox2*, is expressed in the proximal limb bud and deletion of *Shox2* causes a failure of stylopodal element (e.g. femur in the hindlimb) formation. The absence of femur shares phenotypic similarities with the defects observed in the *Tbx4* mutants we report here although girdle elements, which are absent in the *Tbx4* mutant, are spared in the *Shox2* null (Cobb et al. 2006, Yu et al. 2007). We observe downregulation of *Shox2* in the *Tbx4* mutant at E10.5 (Supp. Fig.4G,H) consistent with *Shox2* being a target of *Tbx4* (Glaser et al. 2014) and that this may contribute to the absence of femur in the *Tbx4* mutant. Interestingly, however, by E11.5 the proximal domain of *Shox2* is established in the *Tbx4* mutant (Supp. Fig.4I,J), therefore although *Tbx4* is required to establish the initial domain of *Shox2* at the correct time, *Tbx4* is not essential to establish and maintain *Shox2* expression at later time points.

Conditional deletion of *Fgf8* in the AER generates proximally biased hindlimb skeletal abnormalities. A model to explain these defects proposes that in the absence of AER-FGF signalling a smaller limb bud emerges but precursors of the proximal segment are more severely affected due to increased apoptosis in the proximal region (Lewandoski et al. 2000, Mariani et al. 2008, Sun et al. 2002). We compared *Fgf8* expression, the earliest and predominant FGF expressed in the AER (Mariani et al. 2008), in control hindlimb buds and after *Tbx4* conditional deletion (Fig.4G-L). Expression of *Fgf8* is initiated at the same stage (E10) in the control and *Tbx4* mutant embryos (Fig.4G,H), however the *Fgf8* expression domain is restricted to the posterior AER in the mutant. The posterior restriction in the mutant hindlimb is still evident at E10.5 but by E11.5 the domain of *Fgf8* extends to encapsulate the distal extreme of the *Tbx4* mutant hindlimb, which is narrower than the control hindlimb. Therefore, an *Fgf8*-expressing AER forms in the *Tbx4* mutant hindlimb despite being initially posteriorly restricted.

To determine whether the alteration in *Fgf8* expression domain can lead to regionally restricted cell death, as has been suggested previously, we examined cell death directly using whole mount lysotracker red staining and compared control and conditional mutant hindlimbs over a time-course from E10.5-12.5 (Fig.4M-R). The number of cells undergoing cell death detected by lysotracker red are qualitatively comparable between control and *Tbx4* mutant hindlimbs. Elevated levels of lysotracker red staining, as an indicator of cell death, are not observed in the proximal regions of mutant limb buds that could account for the absence of proximal structures.

Taken together, these results show that neither failure of specification of the proximal segment nor loss of AER-FGF expression and resulting increased cell death can explain the proximal bias of the skeletal phenotype. The initial posterior restriction of *Fgf8* expression in the AER seen in the hindlimb bud at E10-10.5 is, in essence, equivalent to removing the anterior AER. In the chick, following removal of the anterior AER digit 1 fails to develop and frequently the radius is absent but posterior and more proximal structures are unaffected (Todt and Fallon 1987). Therefore, the initial disruption of anterior AER *Fgf8* expression in the *Tbx4* mutant hindlimbs can account for the absence digits observed but does not explain the proximal defects.

Sox9-positive chondroprogenitors are present in the proximal *Tbx4* mutant hindlimb

One explanation for the absence of proximal elements is that the pool of chondroprogenitors that give rise to these structures fail at a step of chondrogenesis. To test this hypothesis, we examined the expression of *Sox9,* a marker of committed chondroprogenitors, and *Collagen2a1* (*Col2a1*), an early marker of differentiating chondrocytes (Fig.5A-H). *Sox9*-expressing cells are detected throughout the proximal-distal extent of *Tbx4* mutant limbs and, significantly, are present in the most proximal regions (Fig.5B) where in the equivalent region of the control the precursors of the pelvis and femur can be detected (Fig.5A). At the same stage, in the control, these proximal cells are beginning to express *Col2a1*, however in the *Tbx4* mutant *Col2a1* is barely detectable (compare Fig.5C, D). In contrast in more distal regions at E12.5, the absence of skeletal elements (e.g. fibula and some digits) is associated with a failure to express both *Sox9* and subsequently *Col2a1* indicating that different mechanisms operate in proximal and distal regions leading to loss of structures in the mutant (Fig.5E-H).

To examine the proximally-localised block in chondrogenesis more closely, we analysed Sox9 protein levels by immunostaining in the background of a *Coll2*-GFP reporter line. Sox9-positive chondroprogenitor cells are present in both proximal and more distal parts of the mutant hindlimb at E11.5 (Fig.5J, L), but initial condensations of Col2-positive chondrocytes that eventually form the pelvis, femur and tibia that can be seen in control (Fig.5I, K) are absent in the mutant (Fig.5J, L). By E12.5, in control hindlimbs rods of Col2-positive cells are clearly visible in the forming pelvis, femur and tibia elements (Fig.5M, O), whereas in the mutant only the tibia and a smaller number of dispersed cells in the pelvic region are present (Fig.5N, P). These results indicate that in the *Tbx4* mutant, Sox9-positive chondroprogenitors are present in the proximal limb bud but these cells fail to take the next steps in the chondrogenic programme and do not express Col2a1.

In the absence of *Tbx4*, chondroprogenitors located in the proximal part of the limb bud fail to differentiate into chondrocytes

To investigate which step of the chondrocyte differentiation process is affected in the absence of *Tbx4*, we used the micromass cell culture technique (see Materials and Methods). This system allows limb bud cells to be studied in isolation from the influence of AER signals and the forming vasculature. If cultured *in vitro* under the correct conditions, limb bud cells are able to differentiate to form cartilage nodules that can be stained with Alcian blue (Fig.6A). In *Tbx4* mutant micromass cultures made from the proximal portion of the limb bud there is an almost complete absence of staining (Fig.6B) indicating a failure to form cartilage. In contrast, equivalent cultures produced from the distal portion of *Tbx4* mutant limbs are able to form cartilage nodules, although not as effectively as control samples (Supplementary Fig.5A,B). This demonstrates that proximal cells in the *Tbx4* mutant have a more severe block in their ability to undergo chondrogenesis than distal cells.

We next examined the chondrogenic differentiation programme in *Tbx4* mutants to determine at what point it is disrupted. In the first steps of chondrogenic differentiation, the Sox9-expressing, prechondrogenic mesenchymal cells aggregate and subsequently condense to form compact cell masses that go on to form cartilage (Fig6C-F). *In vitro* differentiation of chondroprogenitors has been shown to depend critically on the density of progenitors present in culture (Ahrens et al. 1977). To assess if the phenotype observed derived from a lower number of progenitors in the harvested limb cells, we quantified the average number of Sox9-expressing cells in culture from day 1 to day 4 of culture (Fig. 6G-H). We observed on day 1 and 2 no statistical difference of number of Sox9-positive progenitors between controls and mutant condition, suggesting that a difference in the initial cell density of progenitors is not the primary cause of the phenotype observed. However, interestingly, the number of Sox9-positive cells decreases from day 3 of culture, concomitantly with the onset of the compaction process. Defects of cell proliferation cannot account for the decreased number of Sox9-positive cells observed in the absence of *Tbx4* expression since comparable numbers of phospho-Histone H3 (PH3)-positive cells are present in both Sox9-positive mutant and control populations (Fig.6H). Quantification of Caspase3 immunostaining shows there is no increase of apoptosis in the mutant cell cultures (Supplementary Fig.5C-E), suggesting that the reduction in the number of Sox9-positive cells is due to chondroprogenitor cells failing to maintain Sox9 expression rather than these cells being lost via cell death.

Two additional Sox factors, *Sox5* and *Sox6*, are co-expressed with *Sox9* during chondrogenic differentiation (Ikeda et al. 2005). These transcription factors act after mesenchymal condensation has occurred and cooperate with Sox9 to activate the *Col2a1* enhancer and allow chondrocyte differentiation (Smits et al. 2001). At day 4 of micromass culture, Sox6/Sox9 co-expressing cells can be detected (Fig.6I-K) but in cultures of *Tbx4* mutant

cells, Sox9-expressing cells do not co-express Sox6 (Fig.6L-N). Similarly, using peanut agglutinin (PNA) to detect condensing cartilage nodules, Sox5 is observed in control cultures (Fig.6O-Q) but is not detected in *Tbx4* mutant cultures even in regions rich for PNA (Fig.6R-T). Therefore, in *Tbx4* mutants, cartilage formation is disrupted at an early stage.

Sox9-positive chondroprogenitors fail to undergo compaction in *Tbx4* mutant cultures

To examine the cellular behaviour of chondrocytes at the earliest stages of chondrocyte condensation when phenotypes have been observed, we produced time-lapse movies of proximal limb micromass cultures from day 1 to early day 4 (84 hours), a time window encompassing the onset of the differentiation process. Cultures were stained with a cytoplasmic dye and low concentration of Hoechst to follow nuclei (see Materials and Methods). In the control proximal cell culture, at day 1, cells have adhered to the plate and have a classic fibroblast-like morphology (supplementary movie 1 and 2). At day 2, subsets of cells change from a flattened morphology, round up and form aggregates with neighbouring cells and appear to loosen their contacts to the substrate. This process of cell aggregation, which is thought to be the first step of the condensation process (Barna and Niswander 2007) and precedes the onset of *Sox9* expression, is observed in both control and *Tbx4* mutant cultures (Fig. 7A-D and supplementary movie 1 and 2). By day 3, in control cultures, cells at the core of aggregates lose their contacts with the dish and lift up creating a void at the base of the forming nodule (Fig.7C, asterisks and supplementary movie 1). In *Tbx4* mutant cultures, at day 3, cells within aggregates maintain their contacts with the dish and compaction of the chondroprogenitors fails to occur (Fig.7D). By day 3, in control cultures, cells in aggregates stop exchanging neighbours as show by their almost parallel motion revealed by manual tracking of cells in aggregates of wild type cultures (Fig.7E, G). In *Tbx4* mutant cultures at day 3, cells within aggregates maintain their contacts with the dish

and continue to change positions in the aggregate, suggesting that they are unable to maintain stable cell-cell adhesion (Fig.5D,F,H).

To further analyse the distinct topography and cellular organisation of micromass cultures, we generated confocal Z stack scans of cultures stained with phalloidin (for F-actin) and DAPI (for nuclei). X and Y axis views (Fig.7I,J) illustrate that the nodule is a raised area of cells within the culture. This is the result of cells at the core of the nodule losing their contacts with the surface of the dish producing an acellular void beneath the nodule. In normal micromass culture, the appearance of an acellular void corresponds to the accumulation of extracellular matrix. The absence of acellular voids in the *Tbx4* mutant micromass cultures could therefore indicate a failure of, or reduction in, the production of ECM. At both the base and top of the culture (Fig.7I and J, respectively), cells of the forming nodule are arranged in a circular pattern with tightly-packed, rounded cells at the centre. In contrast, *Tbx4* mutant cultures remain flat. Cells retain their contacts with the substrate and are arranged randomly (Fig.7K,L). Thus, *Tbx4* mutant cells exhibit defects in the very earliest stages of chondrocyte differentiation, which leads to the failure of cartilage elements to form properly in this region and ultimately results in proximally-biased defects in the hindlimb.

Discussion

Fgf10 expression is regulated by different mechanisms in the forelimbs and hindlimbs

Establishment and maintenance of a positive feedback-loop of FGF signaling between cells of the limb mesenchyme and AER is essential for limb bud outgrowth and elaboration of the proximal-distal sequence of skeletal elements. This is triggered by expression of Fgf10 ligand in nascent forelimbs and hindlimbs. Deletion of *Fgf10* causes a failure of limb bud formation

and absence of almost the entire limb skeleton with the forelimb and hindlimbs being affected similarly. Our results demonstrate that, although *Fgf10* has equivalent roles in both forelimb and hindlimbs, there are differences in how *Fgf10* expression is regulated in each type of limb. In the forelimb, *Tbx5* is exclusively required for *Fgf10* expression. In the *Tbx5* mutant, *Fgf10* expression is not initiated and consequently all forelimb elements fail to form (Rallis et al. 2003). There is not the same requirement for a *Tbx* input in the hindlimb as our results demonstrate that in the absence of *Tbx4*, low levels of *Fgf10* expression are established and ultimately distal hindlimb elements are produced while more proximal elements are missing. Furthermore, we show that following deletion of both *Tbx4* and *Pitx1*, *Fgf10* is not expressed and all hindlimb elements fail to form. We propose a model in which *Pitx1* has dual, separable inputs in the regulation of *Fgf10* (Fig.3F). *Pitx1* positively regulates *Tbx4* that in turn directly regulates *Fgf10*. *Pitx1* also has a *Tbx4*-independent input into the regulation of *Fgf10* that can establish hypomorphic levels of Fgf10 in the *Tbx4* mutant. While *Isl1*/*Ldb* are required for *Fgf10* expression and are still expressed in the *Tbx4*/*Pitx1* double mutant our results demonstrate that they are not sufficient to rescue *Fgf10* expression and we therefore favour a model in which these factors act as obligate co-factors with Tbx4 and Pitx1 to regulate *Fgf10*.

In our *Tbx4* gene deletion/gene replacement assay, both *Tbx4* and *Tbx5* can rescue hindlimb formation equally well and a morphologically indistinguishable hindlimb is formed in each case, consistent with our previous observations that these genes have no role in determining forelimb or hindlimb morphologies in mouse (Duboc and Logan 2011b, Minguillon et al. 2005, Minguillon et al. 2009). Recently in an avian model, the pigeon, cis regulatory alleles mapping to *Tbx5* (and *Pitx1)* have been mapped to loci associated with feathered feet which are believed to represent partial transformations from hindlimb to forelimb identity (Boer et

al. 2019, Domyan et al. 2016). Whether this represents a difference between avians and mammals in how differences between forelimbs and hindlimb morphologies are established remains to be clarified. Significantly, the immediate downstream target of *Tbx4/5*, *Fgf10*, did not produce any detectable rescue of hindlimb formation indicating that *Tbx* targets other than *Fgf10* are required to establish the FGF positive feedback-loop. Previously we have demonstrated that in the forelimb *Tbx5* acts in a feed-forward loop with *Sall4* to establish FGF signaling (Harvey and Logan 2006). Our results are consistent with *Tbx4* acting in an equivalent feed-forward mechanism in the hindlimb.

In the rescue assays, we describe here and have reported previously (Duboc and Logan 2011b, Minguillon et al. 2005, Minguillon et al. 2009) *Tbx4* and *Tbx5* are equally efficient in rescuing either forelimb or hindlimb formation. Therefore, it remains unclear if there is any functional advantage in acquiring the additional inputs of *Pitx1* and *Isl1*/*Ldb*, in addition to *Tbx4*, for the regulation of *Fgf10* in the hindlimb. In the context of limb evolution, these additional regulatory inputs provide alternative targets for modulation such as that described in stickleback pelvic fin reduction (Chan et al. 2010, Infante et al. 2013, Jones et al. 2012, Shapiro et al. 2004) and they enable reduction in pelvic (hindlimb) appendages without the pectoral appendages (forelimb) being affected.

A novel mechanism for proximal, skeletal limb defects

In the absence of *Tbx4* expression, proximal chondroprogenitors expressing Sox9 do not form aggregates *in vitro* but subsequently fail to undergo compaction and further steps of chondrogenesis (Fig.7M). These cells then progressively decrease Sox9 expression levels. Tbx4 could be acting by regulating signalling pathways known to contribute to cartilage formation in the limb. In chick micromass culture, inhibition of BMP signalling results in

failure of compaction of chondroprogenitors, at a stage similar to that affected in the *Tbx4* mutant we report here. Consistent with this, in mouse, BmpR1a and b are required for the expression of *Sox9*, *Sox6* and *Sox5*. In contrast, in the *Tbx4* mutant, we show that *Sox9* expression is induced but not maintained, suggesting *Tbx4* could act downstream of BmpR1 activity. The canonical Wnt pathway can affect chondrogenic differentiation. Following ectopic Wnt expression in chick micromass culture chondrocytes undergo compaction but their differentiation into chondroblasts is blocked (Day et al. 2005, Rudnicki and Brown 1997). Furthermore, conditional deletion of β-catenin in the mouse results in increased Sox9 expression and an increase in the number of chondrocytes, at the expense of osteoblasts (Day et al. 2005). Both of these processes occur after the compaction of chondroprogenitors, the step we see affected in the *Tbx4* mutant, therefore ruling out the Wnt pathway as a mediator of this observed defect. Both *Tbx4* and *Tbx5* are known to contribute to the initiation of *Fgf10* expression in the limb mesenchyme (Hasson et al. 2007, Minguillon et al. 2005, Rallis et al. 2003). FGFs are required for the viability of the chondrogenic precursor pool that give rise to the cartilaginous templates. Our result show no statistically significant increase of cell death both *in vivo* and *in vitro* when *Tbx4* is deleted, suggesting *Tbx4* activity on chondrogenic precursors is independent of FGF signals. In agreement with this observation, mice lacking *Fgf10* do not form limb buds but do form rudimental girdle structures (scapula and pelvis) ((Sekine et al. 1999), Supp. Fig 1). Girdle elements are absent from both *Tbx5* and *Tbx4* mutant mice arguing *Tbx4/*5 but not *Fgf10* activity is required for the formation of these most proximal elements.

Phocomelia is a congenital limb malformation in which the proximal portion of the limb (humerus/femur and girdle) is absent or poorly developed leaving the more distal structures, which are less affected, attached directly to the trunk. Phocomelia can be caused by either genetic mutations or environmental insults. Phocomelia cases also present sporadically and the causes of these cases are often never determined. At least 25 human syndromes can present with phocomelia. Eight of these conditions have a known affected gene association, for example Holt-Oram Syndrome (OMIM 142900) caused by mutations at the *TBX5* gene locus can present with upper limb phocomelia (Bermejo-Sanchez et al. 2011). The abnormalities produced following conditional deletion of both *Tbx4* alleles in the hindlimb are similar to the defects found in human lower limb phocomelia (Bermejo-Sanchez et al. 2011). The most severely affected skeletal elements are also the same as those affected in human Ischiocoxopodopatellar Syndrome (OMIM 147891), an autosomal dominant disorder caused by mutation in the *TBX4* gene. The main clinical features of this syndrome include anomalies of the pelvis and femur, aplastic or hypoplastic patella and anomalies of the feet that are believed to originate from *TBX4* haploinsufficiency (Bongers et al. 2004, Haarman et al. 2019). In addition, TBX4 homozygous null mutations have been reported to lead to posterior amelia with pelvic hypoplasia (Kariminejad et al. 2019). Hindlimb developmental abnormalities, including clubfoot and tibial hemimelia, have also been associated with deletions or missense mutations in PITX1 (Alvarado et al. 2011, Gurnett et al. 2008, Klopocki et al. 2012, Morel et al. 2020, Rosenfeld et al. 2011). Our observations in the mouse model provide explanations for the defects, particularly the pelvic and femur involvement, observed in these different human conditions.

Studies in animal models have provided clues to which steps of the limb development programme are disrupted leading to phocomelia. Following X-Ray irradiation of chick limb bud, a proximally truncated limb forms (Wolpert et al. 1979). A more recent re-examination of this phenotype suggests that it is caused by selective depletion of proximal chondrocytes that undergo cell death following their exposure in a time window when prechodrogenic progenitors commit to differentiation (Galloway et al. 2009). We demonstrate that in the *Tbx4* mutant, levels of cell death do not increase in the proximal compartment during stages preceding or following the events of cartilage condensation and therefore cell death cannot explain the absence of proximal elements.

Significantly, we demonstrate that defects in proximal skeletal elements can result from a failure of proximal Sox9-positive chondroprogenitors to differentiate into chondrocytes (Fig.7M) rather than by increased levels of cell death of limb proximal mesenchymal cells or a disruption in proximal-distal patterning. In a *Gli3;Plzf* mouse mutant, which displays a similar loss of proximal skeletal structures, *Sox9* expression is lost and cell death is restricted to the proximal hindlimb. *Gli3* and *Plzf* are suggested to establish the spatial and temporal distribution of chondrogenic progenitors in the proximal hindlimb in early limb development (Barna et al. 2005). Moreover, *Plzf* has been identified as an upstream regulator of *Sox9* (Djouad et al. 2014), hence this could explain the absence of *Sox9* in the proximal *Gli3;Plzf* mutant hindlimb bud, in contrast to the *Tbx4* conditional mutant we report here. An additional study has identified significant defects in the hindlimb stylopod and zeugopod in a *Sall4;Plzf* double knockout mutants (Chen et al. 2020). More recently, a study identifying thalidomide-dependent interaction mediated through the ubiquitin-ligase, Cerublon (Crbn), has shown Plzf and Sall4 to be degraded following thalidomide treatment, leading to hypoplasia in chicken limbs (Chen et al. 2020, Yamanaka et al. 2021). Yamanaka et al rescue the hypoplastic

phenotype by overexpressing Plzf, which recovers the expression of *Fgf10* and *Fgf8*. This study concludes that species sensitive to thalidomide produce Crbn-dependent teratogenic phenotypes and the resultant effect cannot be simply explained by a single knockout of *Plzf* or *Sall4* in mouse models.

Current models suggest that proximal-distal positional values are specified early during limb bud formation (Dudley et al. 2002, Mercader et al. 2000, Towers et al. 2012) and that the action of FGFs expressed in the AER serve to expand the number of progenitors in the limb segments so that structures differentiate in a proximal to distal sequence as limb bud outgrowth progresses. The two-signal model for proximal-distal limb patterning incorporates a second component and proposes that proximal structures are specified by retinoic acid from the flank. Outgrowth of the limb bud takes cells out of the range of the proximal source of RA allowing FGFs from the AER to specify distal structures and maintain cell survival (Rosello-Diez et al. 2014, Rosello-Diez et al. 2011, Towers et al. 2012). Our results demonstrate that the proximal-distal markers *Meis1*, *HoxA11* and *Hoxa13,* are expressed in the *Tbx4* mutant and therefore that the phocomelia that develops is not caused by disruption of proximal-distal patterning and a failure to specify proximal cell fates.

To explain the occurrence of phocomelia in *Fgf8* null mice, it has been proposed that all three segments of the limb bud have reduced proportions due to the smaller limb bud size but that the proximal domain is reduced even further by elevated levels of proximal cell death due to decreased AER-FGF signalling. Ultimately, since proximal progenitors have less time to expand before condensation occurs, the femur is more severely compromised than other elements (Mariani et al. 2008). Since *Tbx4* is required for normal expression of *Fgf10* in the mesenchyme, which in turn is necessary to induce *Fgf8* in the overlying ectoderm it is

conceivable that hypomorphic levels of FGF signalling could contribute to the emergence of phocomelia. *Tbx4* and *Tbx5* are only required for the initial induction of *Fgf10* expression and subsequent establishment of the FGF positive-feedback signalling loop but are dispensable for further limb outgrowth (Hasson et al. 2007, Minguillon et al. 2005, Naiche and Papaioannou 2007). Deletion of *Tbx4* at later limb bud stages using the *Prx1Cre* line also produces proximally truncated limbs (Naiche and Papaioannou 2007), suggesting that disrupted FGF signalling might not be the explanation for this phenotype and instead it arises through a block in chondrogenesis as we describe here.

Materials and Methods

Embryos and mouse lines

Mouse embryos were staged according to (Kaufman 1992). Noon on the day a vaginal plug was observed was taken to be E0.5 days of development. The *Tbx4*$^{lox/lox}$ (Naiche and Papaioannou 2007), *Pitx1*$^{-/-}$ (Szeto et al. 1999), *Fgf10*$^{-/-}$(Sekine et al. 1999), *Prrx1-Tbx4*, *Prrx1-Tbx5* (Minguillon et al. 2009), *Col2*-GFP (Cho et al. 2001) have all been described previously. The *Z/EGFgf10* and *RetRV5Cre* deleter transgenic lines were generated by the Procedural Services Section, NIMR (see Supplementary Fig.1, 3).

Skeletal Preparations

The cartilage and bone elements of mouse embryos were stained with Alcian blue and Alizarin red respectively, essentially as previously described (Hogan 1994). The numbers of samples processed were the following: E17.5 control (n=7), *Tbx4*$^{lox/lox}$;*RetRV5Cre* (n=7), *Tbx4*$^{\Delta/lox}$;*RetRV5Cre* (n=3), *Pitx1*$^{-/-}$ (n=7), *Pitx1*$^{-/-}$;*Tbx4*$^{lox/lox}$;*RetRV5Cre* (n=2),

Tbx4$^{lox/lox}$*;RetRV5Cre;Prrx1-Tbx4* (n=3), *Tbx4*$^{lox/lox}$*;RetRV5Cre;Z/EGFgf10* (n=5), *Tbx4*$^{lox/lox}$*;RetRV5Cre;Z/EGFgf10* (n=5), *Tbx4*$^{lox/lox}$*;RetRV5Cre;Prrx1-Tbx5* (n=6), *Fgf10*$^{-/-}$ (n=1), *Fgf10*$^{-/-}$*;RetRV5Cre;Z/EGFgf10* (n=2)

RNA *In situ* hybridisation

Whole mount and section *in situ* hybridisation protocol and *Tbx4, Pitx1, Hoxa13* probes have been described previously (DeLaurier et al. 2006, Riddle et al. 1993), *Fgf10* probe (Bellusci et al. 1997), *Col2a1* probe (Metsaranta et al. 1991), *Sox9* probe (Kent et al. 1996), *Fgf8* (Mahmood et al. 1995). *Islet1,* and *Hoxa11* probes were generated from I.M.A.G.E clones; *Ils1*: IRCLp5011A0814D, I.M.A.G.E ID 40130540, *HoxA11* IRCLp5011D086D, I.M.A.G.E ID 8734051. *Meis1a* (Capdevila et al. 1999, Mercader et al. 2000). Numbers of embryos processed with each probe is described in the respective figure legends.

Whole-mount immunohistochemistry

Immunohistochemistry was performed as previously described (DeLaurier et al. 2006) and tile Z-scanned by confocal microscope (MPSP5, Leica) using a 20x magnification water-dipping lens (Numerical aperture 1.0, Leica 507701). The resulting images were analysed using Fiji (ImageJ) and Volocity (6.1.1, Perkin Elmer Inc.) software. Prior to confocal imaging, embryos were cleared using Clear^{T2} as described (Kuwajima et al. 2013). Sox9 protein was detected using anti-human SOX9-NL557 (R and D, NL3075R).

Lysotracker red

Embryos were dissected in HBS (Hank's balanced salt solution) and placed in 5µl/ml of Lysotracker Red (Invitrogen L7528) for 45 minutes at 37°C. Embryos were then washed 3 times for 10 minutes rocking at room temperature then fixed in 4% paraformaldehyde in PBS

overnight. Rinsed embryos were then cleared and imaged using a Zeiss LSM5 Pascal confocal microscope.

Micromass cultures

Micromass cultures were prepared as previously described (Ahrens et al. 1977, Bruce et al. 2010) from samples of pooled limbs. Hindlimbs were harvested from 11.5 d.p.c. *Tbx4*$^{lox/lox}$*;RetRV5Cre* conditional mutants and wild-type embryos. Hindlimb buds dissected from the flank of the embryo were bisected, transversely at the approximate proximal-distal midpoint to generate proximal and distal portions that were processed separately. Limbs and limb portions were dissociated in 1 unit/ml of dispase II (Roche Diagnostics) solution containing 10% fetal bovine serum (FBS)/Puck's saline A buffer for 20min at 37 °C. Digested limbs were dissociated in growth medium (advanced DMEM/F-12 1:1 medium containing 10% FBS-gold, glutaMAX, Penicillin (25 units/ml), Streptavidin (25 µg/ml) antibiotics, Invitrogen), passed through a 40-µm cell strainer to obtain a single cell suspension, and briefly centrifuged. Cells were resuspended in growth medium at a concentration of 2.5×10^5 cells/ml and spotted in 10µl droplets on Nunclon Delta surface culture dishes. After cells adhered to culture dishes for 1h at 37 °C in a humidified atmosphere containing 5% CO2, medium was added. Growth medium was replaced every two days.

Staining and immunostaining of micromass cultures

For Alcian blue staining, micromass cultures (control proximal culture (n=14) *Tbx4*$^{lox/lox}$*;RetRV5Cre* proximal culture (n=11), control distal culture (n=6), *Tbx4*$^{lox/lox}$*;RetRV5Cre* distal culture (n=6)) were fixed in 4% paraformaldehyde for 30 min then washed briefly in PBS and incubated in 0.1% Alcian blue GX (Sigma) in 0.1 N HCl, pH 1.0, overnight at room temperature. Cultures were cleared in 70% ethanol before images were

captured on a stereomicroscope. For immunostaining, micromass cultures were fixed for 15 min, washed in PBS, blocked in PBS-10% sheep serum. Antibodies were added overnight in blocking solution. Anti-human SOX9-NL557 antibody (R&D systems NL3075R), anti-Sox6 antibody (Abcam ab30455), anti-Sox5 antibody (Santa Cruz sc-17329), PNA-FITC (Sigma L7381), anti-phophohistone H3 (Abcam ab10543), Anti-activated Caspase 3 (Abcam ab32351) and Alexa Fluor® 647 phalloidin (Molecular Probes A22287) used at (50 µg/ml). Immunostained cultures were Z-scanned by confocal microscope (MP-SP5, Leica) using a 20x magnification water-dipping lens (Numerical aperture 1.0, Leica 507701). The resulting images were analysed and cell numbers and volumes were obtained using velocity (6.1.1, Perkin Elmer Inc.). Multi-channel stacks were processed on Volocity for 3D rendering and subsequently volume quantification and cell counting. For each field of view (775x775 µM) (8 fields in total representing 2 different biological repeats for each condition and culture day), to perform segmentation and automated cell counting, we used the following protocol: velocity measurements: find objects using intensity>exclude objects touching edge of image> exclude objects by size. The overlaps between the population of PH3 and Sox9-expressing cells was then assessed. Statistical analysis (mean, s.e.m. and T-test) was performed using Excel (Microsoft).

Cell labelling and live imaging of micromass cultures

One day micromass cultures were incubated in Cell tracker dye (Invitrogen Molecular Probes, CMTPX, C34552) diluted at a final concentration of 2.5µM in pre-warmed DPBS (GIBCO, Invitrogen 14287080) for 30 minutes at 37°C. Hoechst (1 µg/ml) was used to label nuclei by incubating the cells for the last 5 minutes of the 30 minutes incubation. Cells were placed in fresh media and incubated for one hour prior to imaging. Movies are time lapse of Z-scan stacks (1.5 µm steps, 30 µm thick) imaged every 5 minutes using a MPSP5 (Leica)

confocal microscope using a 20x magnification water-dipping lens (Numerical aperture 1.0, Leica 507701) equipped with cell culture chamber. Wild type, control cultures and mutant cultures (*Tbx4*$^{lox/lox}$*;RetRV5Cre)* were imaged concomitantly in the same petri dish (60 mm Nunclon delta surface). Tracking of cells in movies was performed manually using IMARIS 8.2.0 (Bitplane] for 80 frames (7H15m) before the onset of cell compaction.

Competing Interests

The authors declare no competing or financial interest.

Funding

This work was funded by MRC grants MC PC 13052 and MR/S000038/1 to MPOL.

References:

Ahrens PB, Solursh M, Reiter RS. 1977. Stage-related capacity for limb chondrogenesis in cell culture. Dev Biol 60:69-82.
Alvarado DM, McCall K, Aferol H, Silva MJ, Garbow JR, Spees WM, Patel T, Siegel M, Dobbs MB, Gurnett CA. 2011. Pitx1 haploinsufficiency causes clubfoot in humans and a clubfoot-like phenotype in mice. Hum Mol Genet 20:3943-3952.
Barna M, Niswander L. 2007. Visualization of cartilage formation: insight into cellular properties of skeletal progenitors and chondrodysplasia syndromes. Dev Cell 12:931-941.
Barna M, Pandolfi PP, Niswander L. 2005. Gli3 and Plzf cooperate in proximal limb patterning at early stages of limb development. Nature 436:277-281.
Bellusci S, Grindley J, Emoto H, Itoh N, Hogan BL. 1997. Fibroblast growth factor 10 (FGF10) and branching morphogenesis in the embryonic mouse lung. Development 124:4867-4878.
Bermejo-Sanchez E, et al. 2011. Phocomelia: a worldwide descriptive epidemiologic study in a large series of cases from the International Clearinghouse for Birth Defects Surveillance and Research, and overview of the literature. Am J Med Genet C Semin Med Genet 157C:305-320.
Boer EF, Van Hollebeke HF, Park S, Infante CR, Menke DB, Shapiro MD. 2019. Pigeon foot feathering reveals conserved limb identity networks. Dev Biol.
Bongers EM, et al. 2004. Mutations in the human TBX4 gene cause small patella syndrome. Am J Hum Genet 74:1239-1248.
Bruce SJ, Butterfield NC, Metzis V, Town L, McGlinn E, Wicking C. 2010. Inactivation of Patched1 in the mouse limb has novel inhibitory effects on the chondrogenic program. J Biol Chem 285:27967-27981.
Burke AC, Nelson CE, Morgan BA, Tabin C. 1995. Hox genes and the evolution of vertebrate axial morphology. Development 121:333-346.
Capdevila J, Tsukui T, Rodriquez Esteban C, Zappavigna V, Izpisua Belmonte JC. 1999. Control of vertebrate limb outgrowth by the proximal factor Meis2 and distal antagonism of BMPs by Gremlin. Mol Cell 4:839-849.

Chan YF, et al. 2010. Adaptive evolution of pelvic reduction in sticklebacks by recurrent deletion of a Pitx1 enhancer. Science 327:302-305.
Chen KQ, Tahara N, Anderson A, Kawakami H, Kawakami S, Nishinakamura R, Pandolfi PP, Kawakami Y. 2020. Development of the Proximal-Anterior Skeletal Elements in the Mouse Hindlimb Is Regulated by a Transcriptional and Signaling Network Controlled by. Genetics 215:129-141.
Cho JY, Grant TD, Lunstrum GP, Horton WA. 2001. Col2-GFP reporter mouse--a new tool to study skeletal development. Am J Med Genet 106:251-253.
Cobb J, Dierich A, Huss-Garcia Y, Duboule D. 2006. A mouse model for human short-stature syndromes identifies Shox2 as an upstream regulator of Runx2 during long-bone development. Proc Natl Acad Sci U S A 103:4511-4515.
Day TF, Guo X, Garrett-Beal L, Yang Y. 2005. Wnt/beta-catenin signaling in mesenchymal progenitors controls osteoblast and chondrocyte differentiation during vertebrate skeletogenesis. Dev Cell 8:739-750.
DeLaurier A, Schweitzer R, Logan M. 2006. Pitx1 determines the morphology of muscle, tendon, and bones of the hindlimb. Dev Biol 299:22-34.
Djouad F, Tejedor G, Toupet K, Maumus M, Bony C, Blangy A, Chuchana P, Jorgensen C, Noël D. 2014. Promyelocytic leukemia zinc-finger induction signs mesenchymal stem cell commitment: identification of a key marker for stemness maintenance? Stem Cell Res Ther 5:27.
Domyan ET, et al. 2016. Molecular shifts in limb identity underlie development of feathered feet in two domestic avian species. Elife 5:e12115.
Duboc V, Logan MP. 2011a. Pitx1 is necessary for normal initiation of hindlimb outgrowth through regulation of Tbx4 expression and shapes hindlimb morphologies via targeted growth control. Development 138:5301-5309.
---. 2011b. Regulation of limb bud initiation and limb-type morphology. Dev Dyn 240:1017-1027.
Dudley AT, Ros MA, Tabin CJ. 2002. A re-examination of proximodistal patterning during vertebrate limb development. Nature 418:539-544.
Galloway JL, Delgado I, Ros MA, Tabin CJ. 2009. A reevaluation of X-irradiation-induced phocomelia and proximodistal limb patterning. Nature 460:400-404.
Glaser A, Arora R, Hoffmann S, Li L, Gretz N, Papaioannou VE, Rappold GA. 2014. Tbx4 interacts with the short stature homeobox gene Shox2 in limb development. Dev Dyn 243:629-639.
Gurnett CA, Alaee F, Kruse LM, Desruisseau DM, Hecht JT, Wise CA, Bowcock AM, Dobbs MB. 2008. Asymmetric lower-limb malformations in individuals with homeobox PITX1 gene mutation. Am J Hum Genet 83:616-622.
Haarman MG, Kerstjens-Frederikse WS, Berger RMF. 2019. The ever-expanding phenotypical spectrum of human TBX4 mutations: from toe to lung. Eur Respir J 54.
Harvey SA, Logan MP. 2006. sall4 acts downstream of tbx5 and is required for pectoral fin outgrowth. Development 133:1165-1173.
Hasson P, Del Buono J, Logan MP. 2007. Tbx5 is dispensable for forelimb outgrowth. Development 134:85-92.
Hogan BL, Beddington, R. and Costantini, F. 1994. Manipulating the Mouse Embryo: A Laboratory Manual. Cold Spring Harbor Laboratory Press.
Ikeda T, Kawaguchi H, Kamekura S, Ogata N, Mori Y, Nakamura K, Ikegawa S, Chung UI. 2005. Distinct roles of Sox5, Sox6, and Sox9 in different stages of chondrogenic differentiation. J Bone Miner Metab 23:337-340.

Infante CR, Park S, Mihala AG, Kingsley DM, Menke DB. 2013. Pitx1 broadly associates with limb enhancers and is enriched on hindlimb cis-regulatory elements. Dev Biol 374:234-244.
Itou J, Kawakami H, Quach T, Osterwalder M, Evans SM, Zeller R, Kawakami Y. 2012. Islet1 regulates establishment of the posterior hindlimb field upstream of the Hand2-Shh morphoregulatory gene network in mouse embryos. Development 139:1620-1629.
Jones FC, et al. 2012. The genomic basis of adaptive evolution in threespine sticklebacks. Nature 484:55-61.
Kariminejad A, et al. 2019. Homozygous Null TBX4 Mutations Lead to Posterior Amelia with Pelvic and Pulmonary Hypoplasia. Am J Hum Genet 105:1294-1301.
Kaufman MH. 1992. The Atlas of Mouse Development. Elsevier.
Kawakami Y, et al. 2011. Islet1-mediated activation of the beta-catenin pathway is necessary for hindlimb initiation in mice. Development 138:4465-4473.
Kent J, Wheatley SC, Andrews JE, Sinclair AH, Koopman P. 1996. A male-specific role for SOX9 in vertebrate sex determination. Development 122:2813-2822.
Klopocki E, et al. 2012. Deletions in PITX1 cause a spectrum of lower-limb malformations including mirror-image polydactyly. Eur J Hum Genet 20:705-708.
Kuwajima T, Sitko AA, Bhansali P, Jurgens C, Guido W, Mason C. 2013. ClearT: a detergent- and solvent-free clearing method for neuronal and non-neuronal tissue. Development 140:1364-1368.
Lewandoski M, Sun X, Martin GR. 2000. Fgf8 signalling from the AER is essential for normal limb development. Nat Genet 26:460-463.
Logan M, Martin JF, Nagy A, Lobe C, Olson EN, Tabin CJ. 2002. Expression of Cre Recombinase in the developing mouse limb bud driven by a Prxl enhancer. Genesis 33:77-80.
Logan M, Simon HG, Tabin C. 1998. Differential regulation of T-box and homeobox transcription factors suggests roles in controlling chick limb-type identity. Development 125:2825-2835.
Mahmood R, Bresnick J, Hornbruch A, Mahony C, Morton N, Colquhoun K, Martin P, Lumsden A, Dickson C, Mason I. 1995. A role for FGF-8 in the initiation and maintenance of vertebrate limb bud outgrowth. Curr Biol 5:797-806.
Marcil A, Dumontier E, Chamberland M, Camper SA, Drouin J. 2003. Pitx1 and Pitx2 are required for development of hindlimb buds. Development 130:45-55.
Mariani FV, Ahn CP, Martin GR. 2008. Genetic evidence that FGFs have an instructive role in limb proximal-distal patterning. Nature 453:401-405.
Mercader N, Leonardo E, Piedra ME, Martinez AC, Ros MA, Torres M. 2000. Opposing RA and FGF signals control proximodistal vertebrate limb development through regulation of Meis genes. Development 127:3961-3970.
Metsaranta M, Toman D, De Crombrugghe B, Vuorio E. 1991. Specific hybridization probes for mouse type I, II, III and IX collagen mRNAs. Biochim Biophys Acta 1089:241-243.
Minguillon C, Del Buono J, Logan MP. 2005. Tbx5 and Tbx4 are not sufficient to determine limb-specific morphologies but have common roles in initiating limb outgrowth. Dev Cell 8:75-84.
Minguillon C, Gibson-Brown JJ, Logan MP. 2009. Tbx4/5 gene duplication and the origin of vertebrate paired appendages. Proc Natl Acad Sci U S A 106:21726-21730.
Morel G, et al. 2020. Mandibular-pelvic-patellar syndrome is a novel PITX1-related disorder due to alteration of PITX1 transactivation ability. Hum Mutat 41:1499-1506.
Naiche LA, Papaioannou VE. 2003. Loss of Tbx4 blocks hindlimb development and affects vascularization and fusion of the allantois. Development 130:2681-2693.
---. 2007. Tbx4 is not required for hindlimb identity or post-bud hindlimb outgrowth. Development 134:93-103.

Narkis G, Tzchori I, Cohen T, Holtz A, Wier E, Westphal H. 2012. Isl1 and Ldb co-regulators of transcription are essential early determinants of mouse limb development. Dev Dyn 241:787-791.
Nishimoto S, Logan MP. 2016. Subdivision of the lateral plate mesoderm and specification of the forelimb and hindlimb forming domains. Semin Cell Dev Biol 49:102-108.
Nishimoto S, Wilde SM, Wood S, Logan MP. 2015. RA Acts in a Coherent Feed-Forward Mechanism with Tbx5 to Control Limb Bud Induction and Initiation. Cell Rep 12:879-891.
Novak A, Guo C, Yang W, Nagy A, Lobe CG. 2000. Z/EG, a double reporter mouse line that expresses enhanced green fluorescent protein upon Cre-mediated excision. Genesis 28:147-155.
Rallis C, Bruneau BG, Del Buono J, Seidman CE, Seidman JG, Nissim S, Tabin CJ, Logan MP. 2003. Tbx5 is required for forelimb bud formation and continued outgrowth. Development 130:2741-2751.
Riddle RD, Johnson RL, Laufer E, Tabin C. 1993. Sonic hedgehog mediates the polarizing activity of the ZPA. Cell 75:1401-1416.
Rosello-Diez A, Arques CG, Delgado I, Giovinazzo G, Torres M. 2014. Diffusible signals and epigenetic timing cooperate in late proximo-distal limb patterning. Development 141:1534-1543.
Rosello-Diez A, Ros MA, Torres M. 2011. Diffusible signals, not autonomous mechanisms, determine the main proximodistal limb subdivision. Science 332:1086-1088.
Rosenfeld JA, et al. 2011. Deletions and duplications of developmental pathway genes in 5q31 contribute to abnormal phenotypes. Am J Med Genet A 155A:1906-1916.
Rudnicki JA, Brown AM. 1997. Inhibition of chondrogenesis by Wnt gene expression in vivo and in vitro. Dev Biol 185:104-118.
Sekine K, et al. 1999. Fgf10 is essential for limb and lung formation. Nat Genet 21:138-141.
Shapiro MD, Marks ME, Peichel CL, Blackman BK, Nereng KS, Jonsson B, Schluter D, Kingsley DM. 2004. Genetic and developmental basis of evolutionary pelvic reduction in threespine sticklebacks. Nature 428:717-723.
Singh P, Schwarzbauer JE. 2012. Fibronectin and stem cell differentiation - lessons from chondrogenesis. J Cell Sci 125:3703-3712.
Smits P, Li P, Mandel J, Zhang Z, Deng JM, Behringer RR, de Crombrugghe B, Lefebvre V. 2001. The transcription factors L-Sox5 and Sox6 are essential for cartilage formation. Dev Cell 1:277-290.
Sukumaran M, Waxman SG, Wood JN, Pachnis V. 2001. Flanking regulatory sequences of the locus encoding the murine GDNF receptor, c-ret, directs lac Z (beta-galactosidase) expression in developing somatosensory system. Dev Dyn 222:389-402.
Sulaiman FA, Nishimoto S, Murphy GR, Kucharska A, Butterfield NC, Newbury-Ecob R, Logan MP. 2016. Tbx5 Buffers Inherent Left/Right Asymmetry Ensuring Symmetric Forelimb Formation. PLoS Genet 12:e1006521.
Sun X, Mariani FV, Martin GR. 2002. Functions of FGF signalling from the apical ectodermal ridge in limb development. Nature 418:501-508.
Szeto DP, Rodriguez-Esteban C, Ryan AK, O'Connell SM, Liu F, Kioussi C, Gleiberman AS, Izpisua-Belmonte JC, Rosenfeld MG. 1999. Role of the Bicoid-related homeodomain factor Pitx1 in specifying hindlimb morphogenesis and pituitary development. Genes Dev 13:484-494.
Todt WL, Fallon JF. 1987. Posterior apical ectodermal ridge removal in the chick wing bud triggers a series of events resulting in defective anterior pattern formation. Development 101:501-515.
Towers M, Wolpert L, Tickle C. 2012. Gradients of signalling in the developing limb. Curr Opin Cell Biol 24:181-187.

Wolpert L, Tickle C, Sampford M. 1979. The effect of cell killing by x-irradiation on pattern formation in the chick limb. J Embryol Exp Morphol 50:175-193.
Yamanaka S, et al. 2021. Thalidomide and its metabolite 5-hydroxythalidomide induce teratogenicity via the cereblon neosubstrate PLZF. EMBO J:e105375.
Yu L, Liu H, Yan M, Yang J, Long F, Muneoka K, Chen Y. 2007. Shox2 is required for chondrocyte proliferation and maturation in proximal limb skeleton. Dev Biol 306:549-559.

Figures

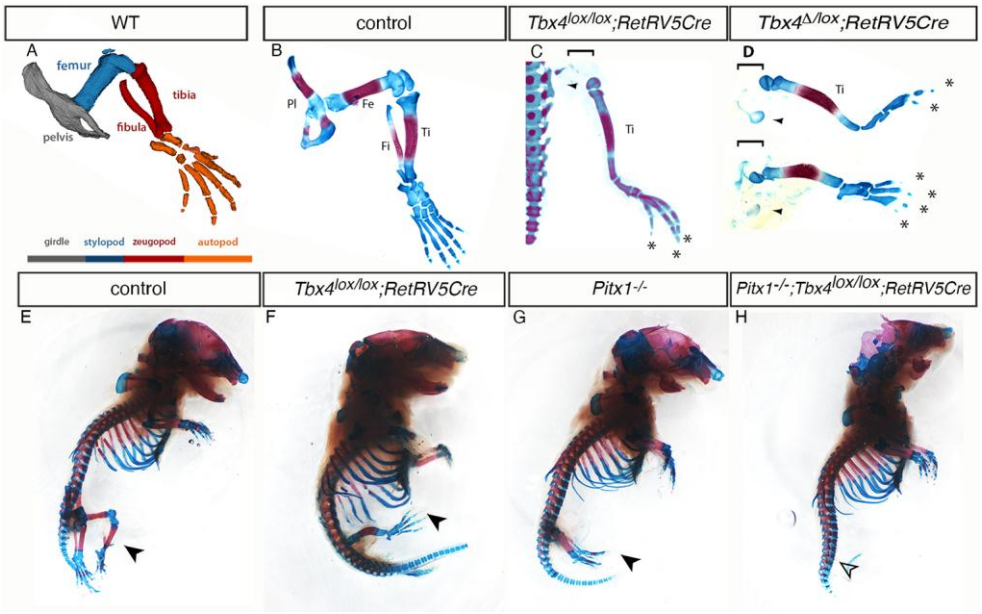

Figure 1: A-D Conditional deletion of *Tbx4* in the hindlimb results in absence of proximal elements and some digits. A, Schematic depicting the three anatomical regions of the limb, Stylopod (blue), zeugopod (red) and autopod (orange) and their composite skeletal elements. **B-D**, Alcian blue/Alizarin red skeletal preparations of E17.5 hindlimbs. **B**, wild-type control (n=7). **C**, *Tbx4*$^{lox/lox}$*;RetRV5Cre* (n=7). **D**, *Tbx4*$^{\Delta/lox}$*;RetRV5Cre* (n=3). Arrowheads point to rudimentary pelvises; brackets show the absence of the femur, asterisks indicate the remaining digits. **E-H *Tbx4* and *Pitx1* are required for hindlimb formation. E-H,** Alcian blue/Alizarin red skeletal preparations of E17.5 embryos. **E,** control wild-type skeleton (n=7)**. F,** *Tbx4*$^{lox/lox}$*;RetRV5Cre* (n=7) **G,** *Pitx1*$^{-/-}$ (n=7) **H,** *Pitx1*$^{-/-}$*;Tbx4*$^{lox/lox}$*;RetRV5Cre* (n=2) black arrowheads indicate the hindlimbs; empty arrowhead indicates the absence of a hindlimb in **H**.

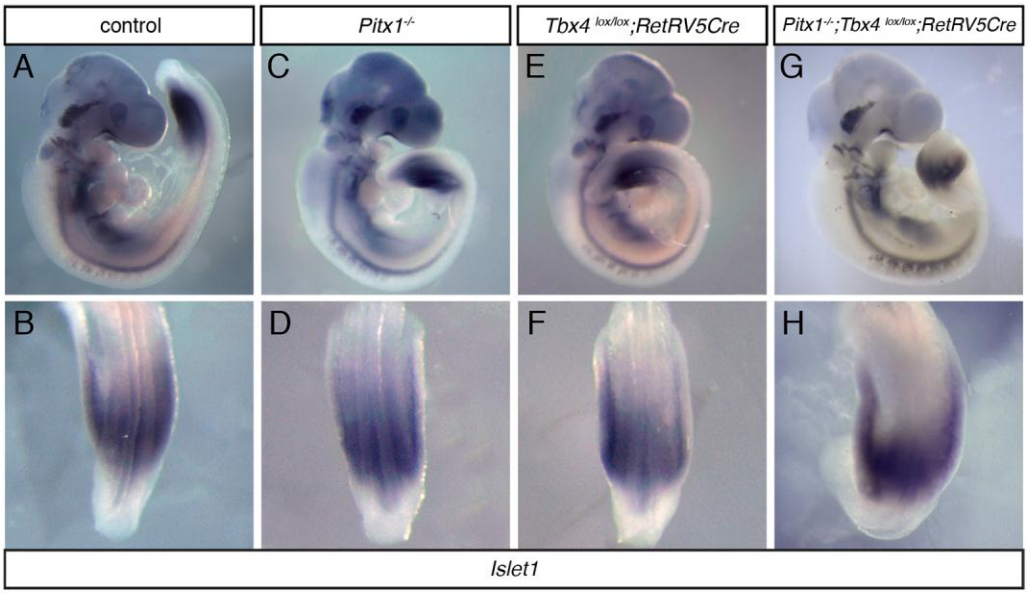

Figure 2: *Tbx4* and *Pitx1* are not required for *Islet1* expression in the hindlimb-forming region. Whole mount *in situ* hybridisation for *IsletI1* expression. Upper panels are lateral views of E9.75 embryos. Lower panel are dorsal views of the caudal end of embryos encompassing the hindlimb-forming region. **A,B**, control embryo (n=11). **C,D** *Pitx1*$^{-/-}$ mutant (n=6). **E,F**, *Tbx4*$^{lox/lox}$*;RetRV5Cre* conditional mutant (n=8)**. G,H,** *Pitx1*$^{-/-}$ *;Tbx4*$^{lox/lox}$*;RetRV5Cre* compound mutant embryos (n=2).

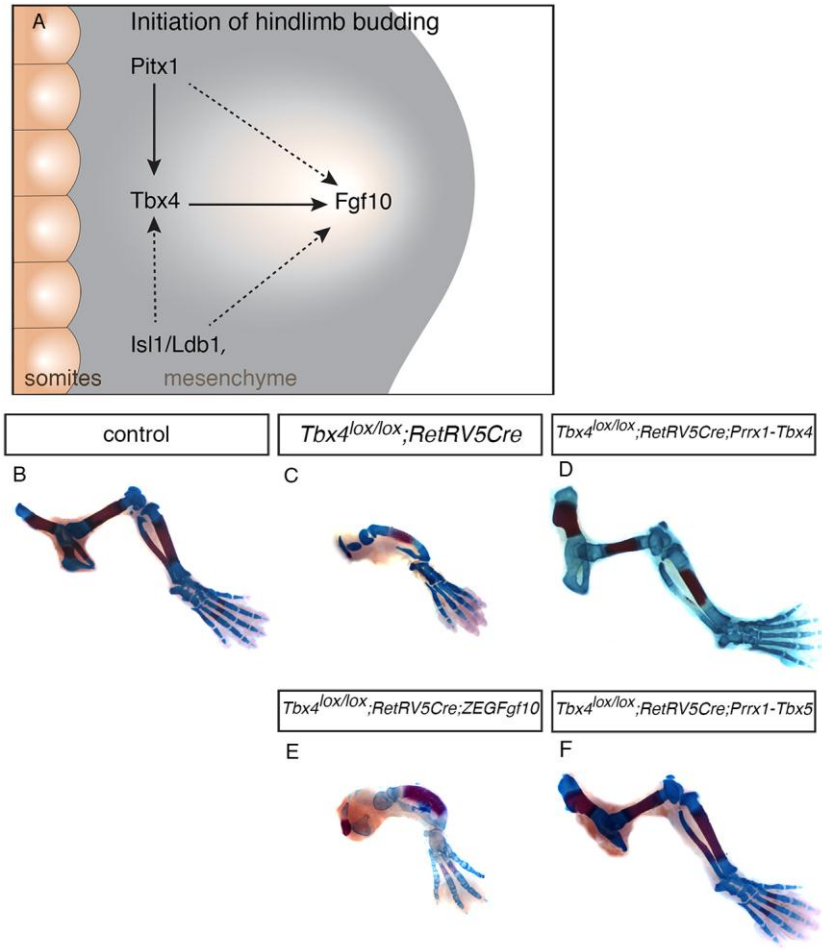

Figure 3: *Tbx5* but not *Fgf10* can rescue hindlimb development in the absence of *Tbx4*. **A,** schematic representation of the gene regulatory network operating during the initiation of hindlimb outgrowth. Alcian blue/Alizarin red skeletal preparation of E17.5 hindlimbs. **B,** control (n=7). **C,** *Tbx4*$^{lox/lox}$*;RetRV5Cre* hindlimb (n=8). **D,** *Tbx4*$^{lox/lox}$*;RetRV5Cre;Prrx1-Tbx4* (n=3) **E**, *Tbx4*$^{lox/lox}$*;RetRV5Cre;Z/EGFgf10* (n=5) **F,** *Tbx4*$^{lox/lox}$*;RetRV5Cre;Prrx1-Tbx5* (n=6)

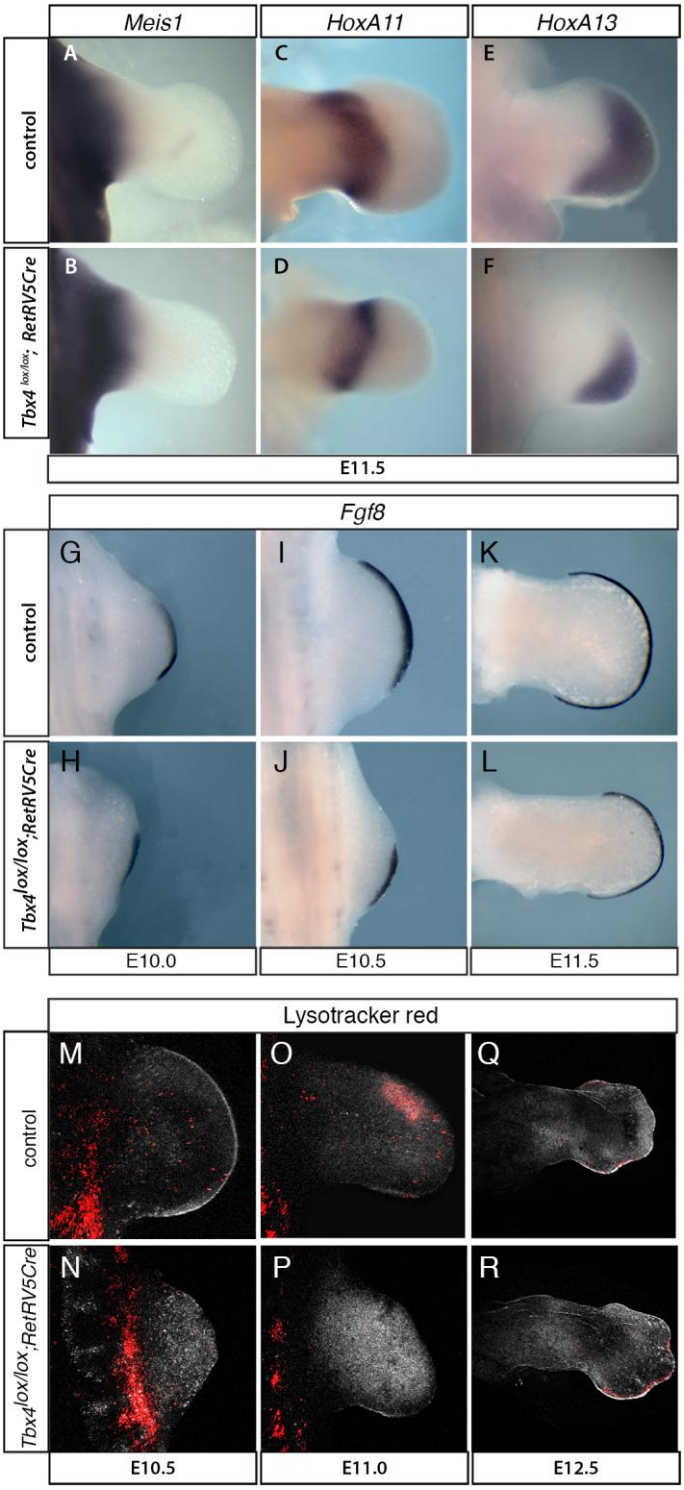

Figure 4: Disruption of proximal-distal patterning, *Fgf8* expression in the AER and elevated levels of cell death are not observed in the *Tbx4* mutant hindlimbs. A-F, Whole mount *in situ* hybridization of E11.5 hindlimbs Upper row wild-type control hindlimbs. Lower row, *Tbx4*$^{lox/lox}$*;RetRV5Cre* mutant hindlimbs. Expression of the proximal segment

(stylopod) marker *Meis1* (n=3) (**A**) is expressed in the mutant (n=3) (**B**). Medial segment (zeugopod) marker *Hoxa11* (n=5) (**C**) is expressed in the *Tbx4* mutant (n=2) (**D**), distal segment (autopod) marker *Hoxa13* (n=3) (**E**) is expressed in the *Tbx4* mutant (n=6) (**F**). **G-L,** Upper row wild-type control hindlimbs. Lower row, $Tbx4^{lox/lox}$*;RetRV5Cre* mutant hindlimbs. Whole mount *in situ* hybridisation for *Fgf8* on control hindlimbs at E10 (n=3) (**G)**, E10.5 (n=3) (**I)**, E11.5 (n=3) (**K)** and $Tbx4^{lox/lox}$*;RetRV5Cre* mutant hindlimbs at E10 (n=2) (**H)** E10.5 (n=3) (**J**) and E11.5 (n=2) (**L**) . **M-R,** Whole mount lysotracker red staining for apoptotic cells, confocal Z-stacks images of control (**M**,**O**,**Q**) and *Tbx4* mutant (**N**,**P**,**R**) hindlimbs. **M,N,** E10.5 **O,P** E11.5 **Q,R** E12.5.

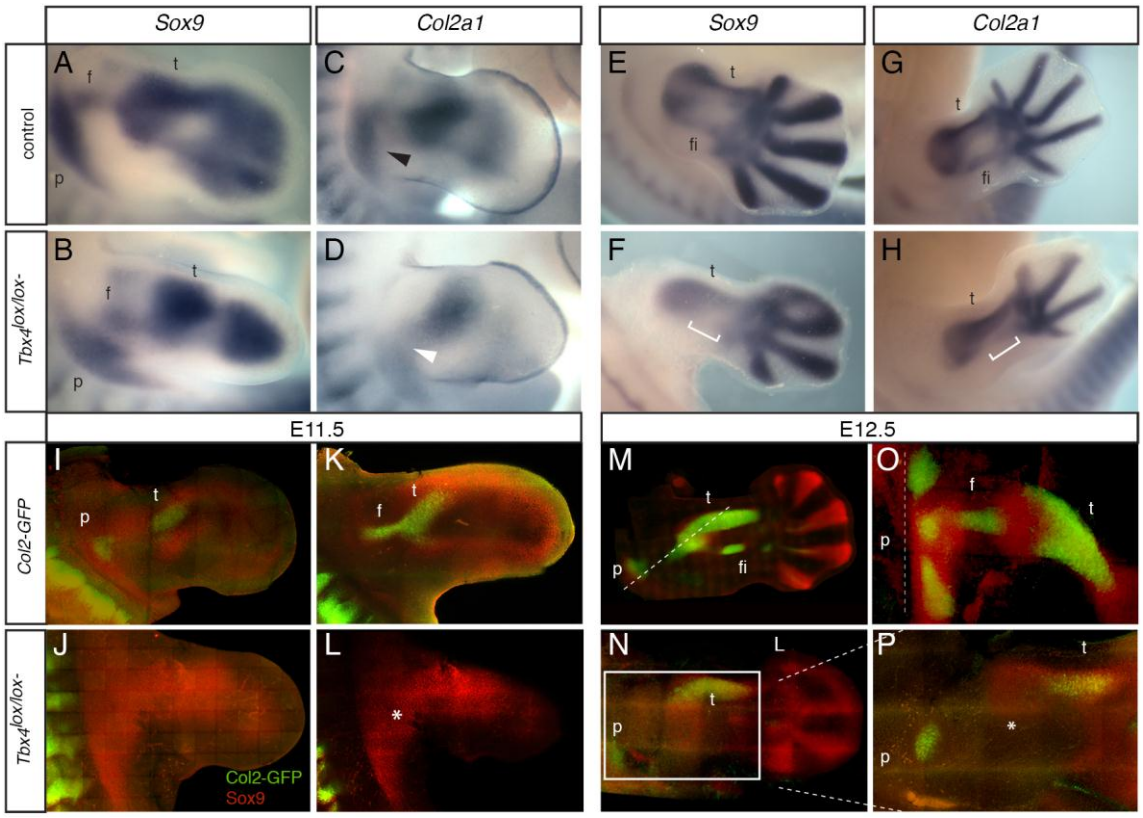

Figure 5: Sox9-expressing chondroprogenitors are present in proximal *Tbx4* mutant hindlimbs but fail to differentiate into chondrocytes. A-H, Whole mount *in situ* hybridisation showing *Sox9* expression in control (n=9) (**A**) and *Tbx4*$^{lox/lox}$;*RetRV5Cre* (n=5) (**B**) hindlimbs at E11.5. *Col2a1* expression in control (n=4) (**C**) and *Tbx4*$^{lox/lox}$;*RetRV5Cre* (n=2) (**D**) hindlimbs. *Sox9* expression in control (n=5) (**E**) and *Tbx4*$^{lox/lox}$;*RetRV5Cre* (n=3) (**F**) hindlimbs at E12.5. *Col2a1* expression in control (n=6) (**G**) and *Tbx4*$^{lox/lox}$;*RetRV5Cre* (n=3) (**H**) hindlimbs. *Col2a1* expression in the pelvic region of the control hindlimb (black arrowhead in **C**) is reduced or absent in the mutant hindlimb (white arrowhead in **D**). **I-P** Whole mount immunostaining for Sox9 (red) chondroprogenitor marker in the background of the *Coll2-GFP* transgenic mouse reporter that labels chondrocytes (green) in the forming cartilage. **I**, **J**, **M**, **N** are 3D renderings of confocal Z-stacks of images, **K**, **L**, **O**, **P** are images of a single Z-plane in the stack. (**I,K)** control-*Coll2GFP* hindlimb at E11.5, with condensation of the forming pelvis (p), femur (f) and tibia (t) annotated. These condensations

are absent from the *Tbx4*$^{lox/lox}$;*RetRV5Cre;Coll2*-GFP hindlimbs (**J**,**L**). The asterisk in (**L**) indicates the proximal pool of chondroprogenitors. (**M**,**O**) Control-*Coll2*GFP hindlimb at E12.5 with pelvis, tibia and fibula (fi) condensations indicated. (**N**,**P**) *Tbx4*$^{lox/lox}$;*RetRV5Cre;Coll2*-GFP hindlimbs. Dashed line in (**M**) and rectangle in (**N**) indicate the plane of Z-section through the limb. Asterisk in (**P**) indicates the absence of femur condensation.

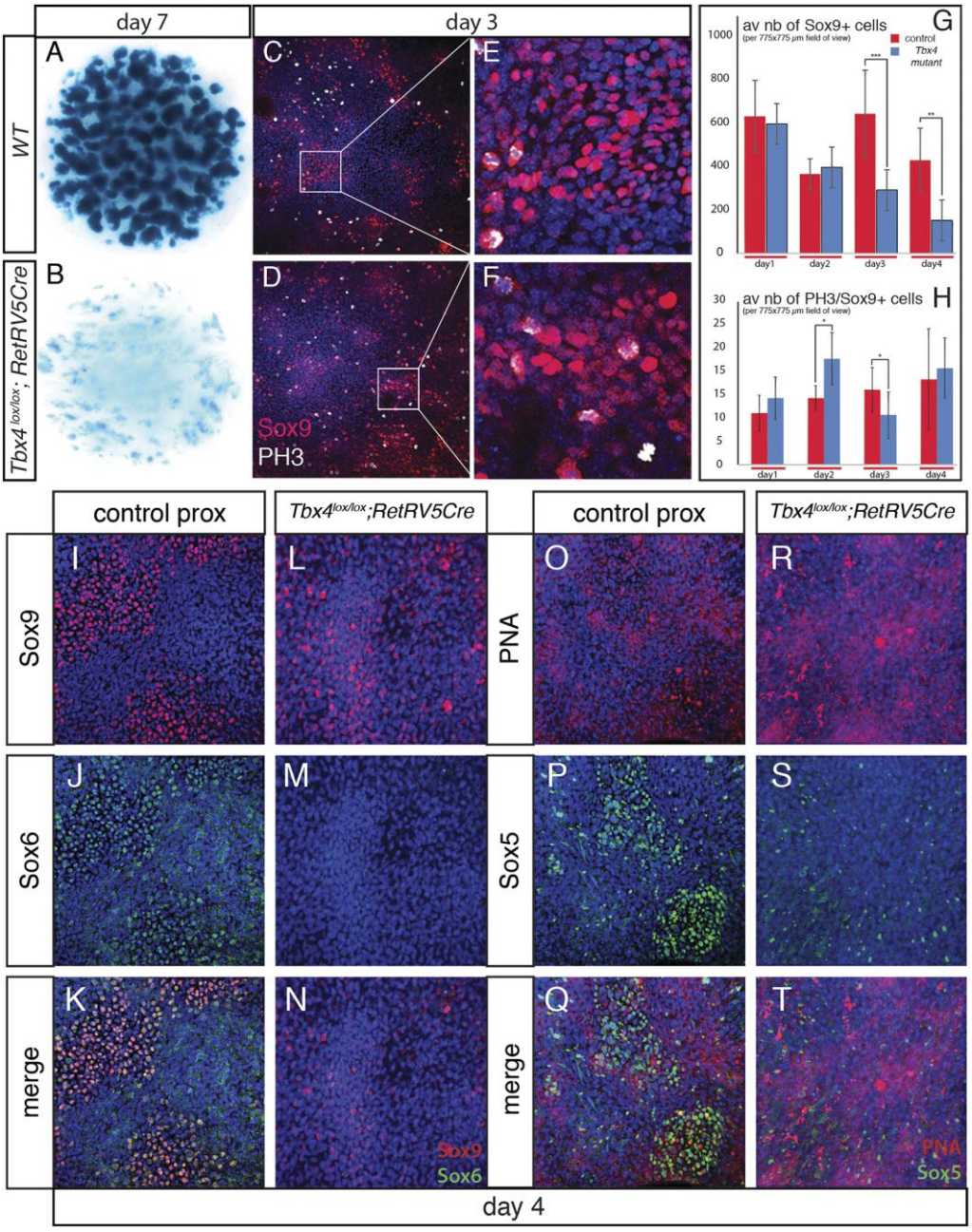

Figure 6: *Tbx4*$^{lox/lox}$*;RetRV5Cre* chondroprogenitors fail to differentiate into chondrocytes. A-B, Alcian blue staining of cartilage nodules in day 7 micromass cultures. (**A**) Control proximal culture (n=14) (**B**) *Tbx4*$^{lox/lox}$*;RetRV5Cre* culture (n=11). **C-F** immunostaining of day 3 proximal limb cultures. Sox9 (red), and DAPI nuclear staining (blue) (**C**) control and (**D**) *Tbx4*$^{lox/lox}$*;RetRV5Cre.* (**E**) higher magnification of a forming nodule (boxed in C) showing rounded Sox9-positive cells. (**F**) higher magnification of

Tbx4$^{lox/lox}$*;RetRVCre5* culture (boxed in D) showing Sox9-positive aggregate of cells that do not have a rounded morphology**. (G)** histogram showing mean ± s.e.m. number of Sox9 expressing cells in control proximal micromass (red) cultures and *Tbx4*$^{lox/lox}$*;RetRV5Cre* proximal culture (blue) per 775x775 µm. These numbers are equivalent at day 1 and progressively decrease as compaction proceeds around day 3 of culture. (**H**) Histogram showing mean ± s.e.m. number of proliferating cells (phospho-Histone H3 (PH3)-expressing) among Sox9 expressing cells from day1 to day4 of culture. **I-T,** Double immunostaining of proximal limb mesenchymal cell cultures (4 days) showing expression of **I,L** Sox9, **J**, **M** Sox6, **K**,**N** merge Sox9 in red, Sox6 in green, nuclear staining (DAPI) in blue on **I-K** WT proximal control (n=3) and **L-N** *Tbx4*$^{lox/lox}$*;RetRV5Cre* proximal culture (n=3) **, O,R** Peanut agglutinin (PNA) a marker of chondroprogenitor cells undergoing condensation (n=3), **P**,**S** Sox5, **Q**,**T** merge Sox5 (green), PNA (red), DAPI nuclear staining (blue) on **O-Q** WT proximal control and **R-T** *Tbx4*$^{lox/lox}$*;RetRV5Cre* proximal culture.

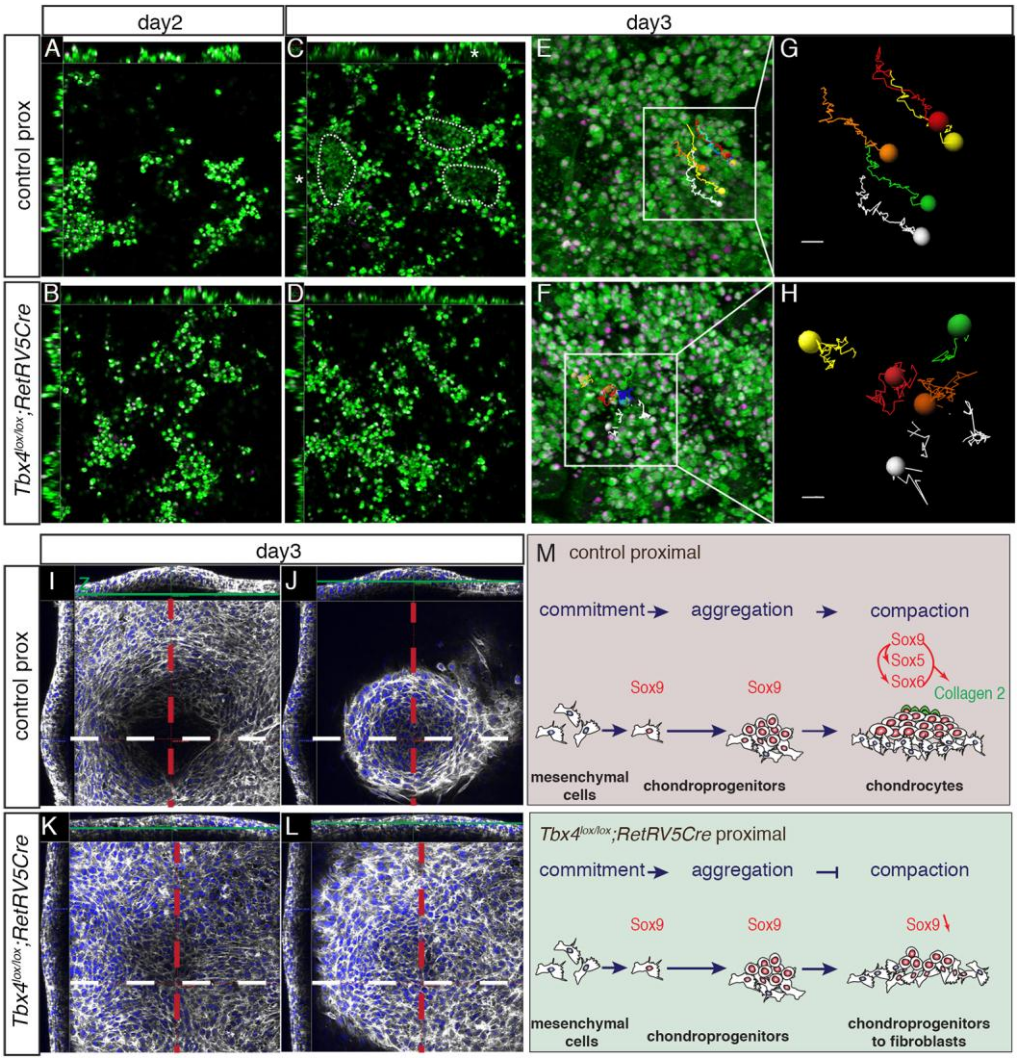

Figure 7: *Tbx4* mutant chondroprogenitors fail to undergo compaction in micromass culture.

Confocal images extracted from a 84 hour time-lapse analysis of control (**A**,**C**,**E**) and *Tbx4* mutant, *Tbx4*$^{lox/lox}$*;RetRV5Cre* (**B**,**D**,**F**) proximal limb bud micromass culture. (**A-D**) X,Y and Z views of the same cultures. Z views in **A-D** are a single scan through approximately the middle of the stack. X and Y views show the entire Z stack along lines though the cultures. At day 2 of culture, both control (**A**) and *Tbx4* mutant (**B**) cultures form cell aggregates. At day 3, cells at the centre of aggregates (**C**) lose their contacts with the substrate and lift off the dish while retaining close contacts with one another. A void is created under the forming

nodule (asterisks) below the centre of the cell aggregate. This behaviour is coincident with the onset of compaction. In *Tbx4* mutant cultures (**D**), cell aggregates maintain connections with the dish, cells fail to lift off the dish and the compaction process is not evident. (**E-F)** extended focus images of Z-stacks showing the area culture were cells were tracked. (**G-H**) 7h15m tracks of cells in wild type (**G**) and *Tbx4* mutant cultures (**H**). (**I-L**) Day 3 cultures stained for nuclei (DAPI, blue) and F-actin (phalloidin, white). Each panel shows confocal X, Y and Z views of focal planes through levels at the base of the culture (**I**,**K**) and top of the culture (**J**,**L**). The control cultures have distinctive features: (**I**) a void forms under the forming nodule. At both the base (**I**) and top of the culture (**J**), cells of the forming nodule are arranged in a circular pattern with tightly-packed, rounded cells at the centre that have lost their contacts with the dish surface. In *Tbx4* mutant cultures (**K-L**) cells are arranged randomly, have retained their contacts to the dish and do not lift off the dish. (**M**) Summary of the chondrocyte differentiation process in control and in *Tbx4*$^{lox/lox}$*;RetRV5Cre* micromass cultures.

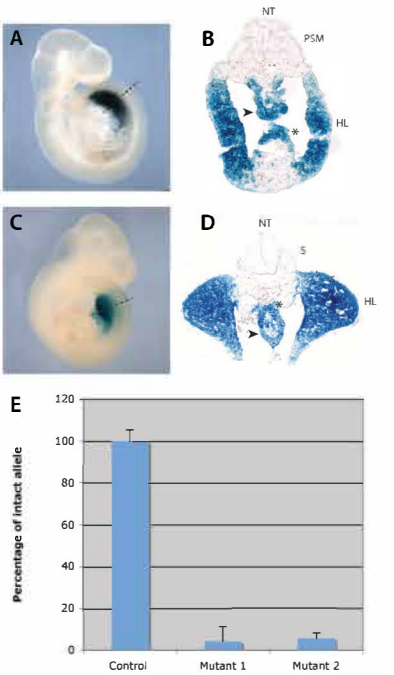

Fig. S1. Cre recombinase activity in the hindlimb-forming LPM in the *RetRV5Cre* transgenic deleter line. LacZ staining of Cre expressing cells at E9.75 (n=8). **(A,C)** right-side lateral views of whole embryos. **(B,D)** Transverse cryosections through the hindlimb regions of embryos. **A,** E9.5 *Rosa26RlacZ;RetRV5Cre* embryo. LacZ activity is detected in the nascent hindlimb bud. **B**, Transverse cryosection through the hindlimb region of an E9.5 *Rosa26RlacZ;RetRV5Cre* embryo. LacZ activity is additionally present in the hindgut diverticulum (black arrowhead) and anterior to the vitelline artery (black asterisk). **C**, E10.5 *Rosa26RlacZ;RetRV5Cre* embryo, LacZ activity is detectable throughout the hindlimb buds. **D**, Transverse cryosection through the hindlimbs of an E10.5 *Rosa26RlacZ;RetRV5Cre* embryo, in which LacZ activity is not detectable in the ectoderm. LacZ activity is visible in the mesoderm of the hindgut (black arrowhead) and the dorsal mesentery (black asterisk). NT–Neural tube, S–somite, PSM–presomitic mesoderm, HL–hindlimb **E**, Graphical representation of Q-PCR results to analyse the extent of deletion of the *Tbx4* conditional allele in 2 separate E10.5 $Tbx4^{lox/lox}$;*RetRV5Cre* hindlimbs . An estimated 96% of conditional *Tbx4* allele has been excised in $Tbx4^{lox/lox}$;*RetRV5Cre* mutant hindlimbs.

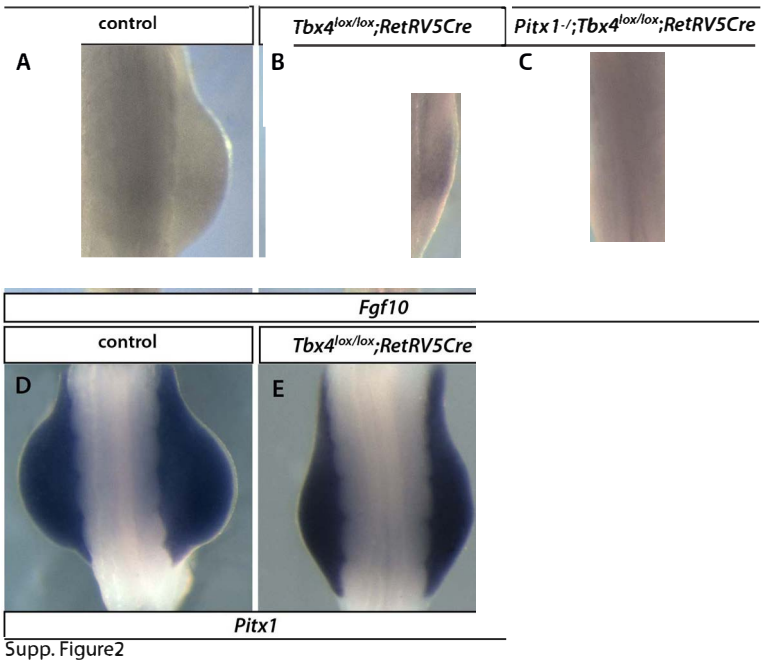

Fig. S2. *Fgf10* expression is regulated by dual inputs from *Tbx4* and *Pitx1*. Whole mount *in situ* hybridisation showing *Fgf10* expression in E10.25 hindlimbs of **A**, control (n=8), **B**, *Tbx4*$^{lox/lox}$;*RetRV5Cre* (n=3) **C**, *Pitx1*$^{-/-}$;*Tbx4*$^{lox/lox}$;*RetRV5Cre* (n=2) **D,E** *Pitx1*

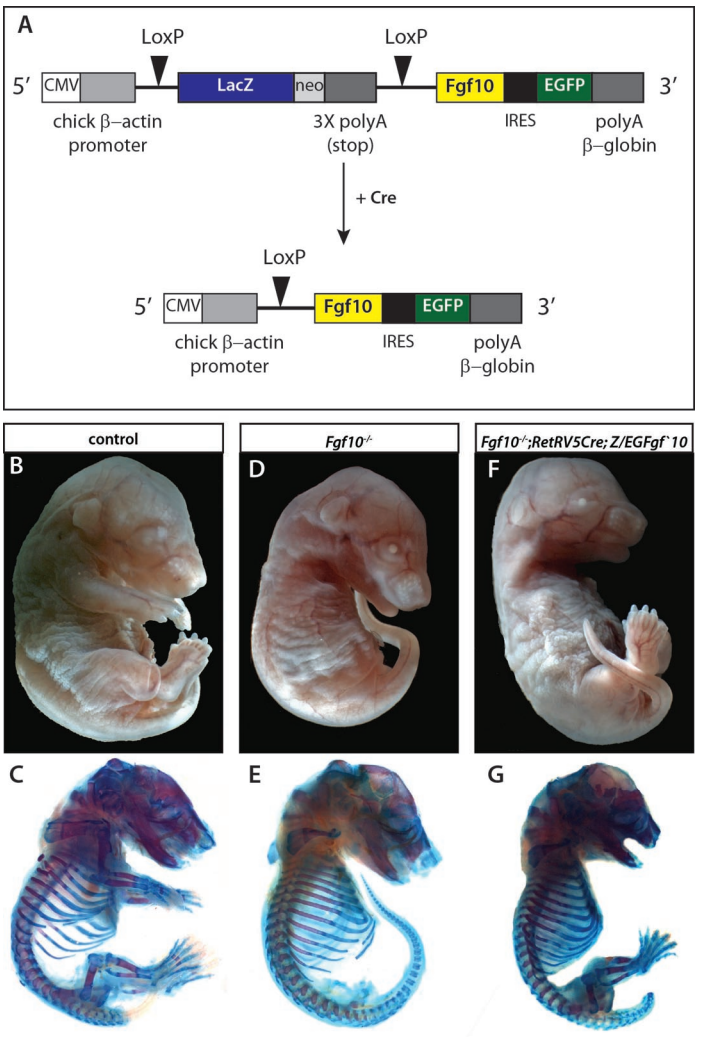

Suppl. Figure3

Fig. S3. The *Z/EGFgf10* transgene is able to fully rescue hindlimb outgrowth in *Fgf10*$^{-/-}$ embryos when activated by the *RetRV5Cre* line. A, Cre recombinase recombines the *LoxP* flanked cassette to enable transgenic *Fgf10* transcription in the *Z/EGFgf10* construct. The *Z/EGFgf10* construct was produced using the *Z/EG* transgenic backbone (Novak et al. 2000) and contains a β-Geo cassette, flanked by two *LoxP* sites (black triangles) downstream of the chick β-actin promoter (light grey rectangle) and the CMV enhancer (white rectangle). The β-Geo cassette contains *LacZ* sequence (blue rectangle) and a neomycin resistance gene (neo), as well as a 3x polyadenylation sites (dark grey) that serve as a transcriptional stop signal. Located 3' of the β -Geo cassette is the *Fgf10* cDNA (yellow rectangle) and an internal ribosome entry site (*IRES*, black rectangle), *eGFP* (green rectangle) and β-globin polyadenylation signal (dark grey rectangle). In the absence of Cre recombinase, CAGGS drives transcription of β-Geo. Following cre excision, the β-Geo cassette is removed and the *Fgf10*/*IRES*/*eGFP* cassette comes under the control of the CAGGS promoter. **B,D,F**, E17.5 embryos and **C,E,G**, complementary skeletal preparation of **B**,**C** control (n=1), **D,E** *Fgf10*$^{-/-}$ (n=1) and **F**,**G** *Fgf10*$^{-/-}$*;RetRV5Cre;Z/EGFgf10* rescued embryos (n=2). Hindlimb formation is completely rescued in the *Fgf10* mutant by activation of the *Fgf10* transgene.

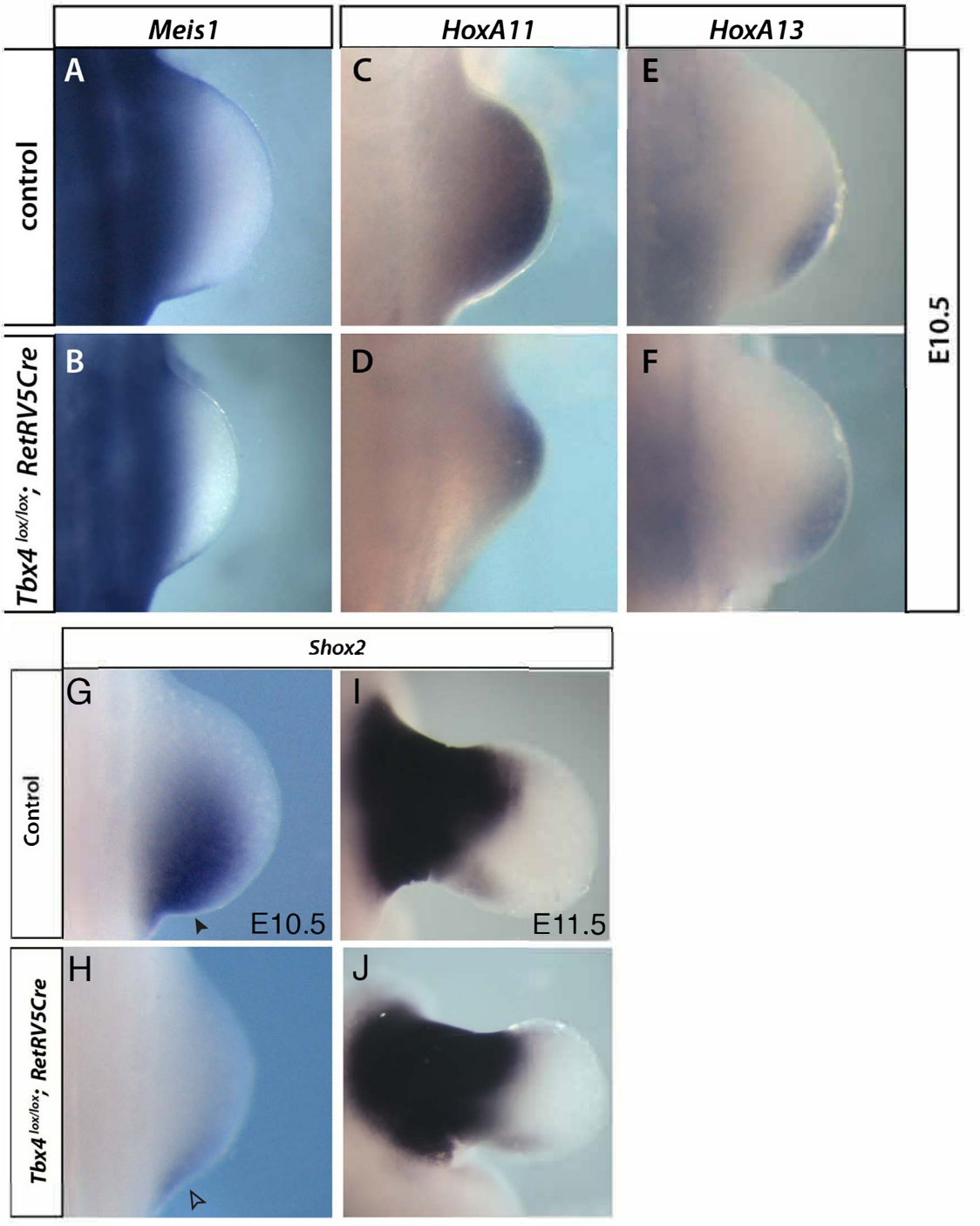

Fig. S4. *Meis1*, *Hoxa11* and *Hoxa13* are expressed in *Tbx4* mutant hindlimb buds. **A-F** Whole mount *in situ* hybridisation of E10.5 hindlimb buds. Dorsal views. Expression of the proximal segment (stylopod) marker *Meis1* (n=3) (**A**) is expressed in the *Tbx4*$^{lox/lox}$*;RetRV5Cre* mutant (n=3) (**B**). Medial segment (zeugopod) marker *Hoxa11* (n=3) (**C**) is expressed in the *Tbx4* mutant (n=2) (**D**). At E10.5 *Hoxa11* is expressed both medially and distally. Distal segment (autopod) marker *Hoxa13* (n=3) (**E**) is expressed in the *Tbx4* mutant (n=3) (**F**). ***Shox2* is downregulated in the *Tbx4* mutant at E10.5** Whole mount *in situ* hybridisation of E10.5 control (n=4) (**G**) and *Tbx4*$^{lox/lox}$*;RetRV5Cre* mutant (n=3) (**H**). Robust expression in control (solid arrow) contrasts with reduced expression in the *Tbx4* conditional mutant (hollow arrow). *Shox2* expression is restricted to the proximal limb bud at E11.5 in control (n=3) (**I**) and *Tbx4*$^{lox/lox}$*;RetRV5Cre* mutant (n=2) (**G**).

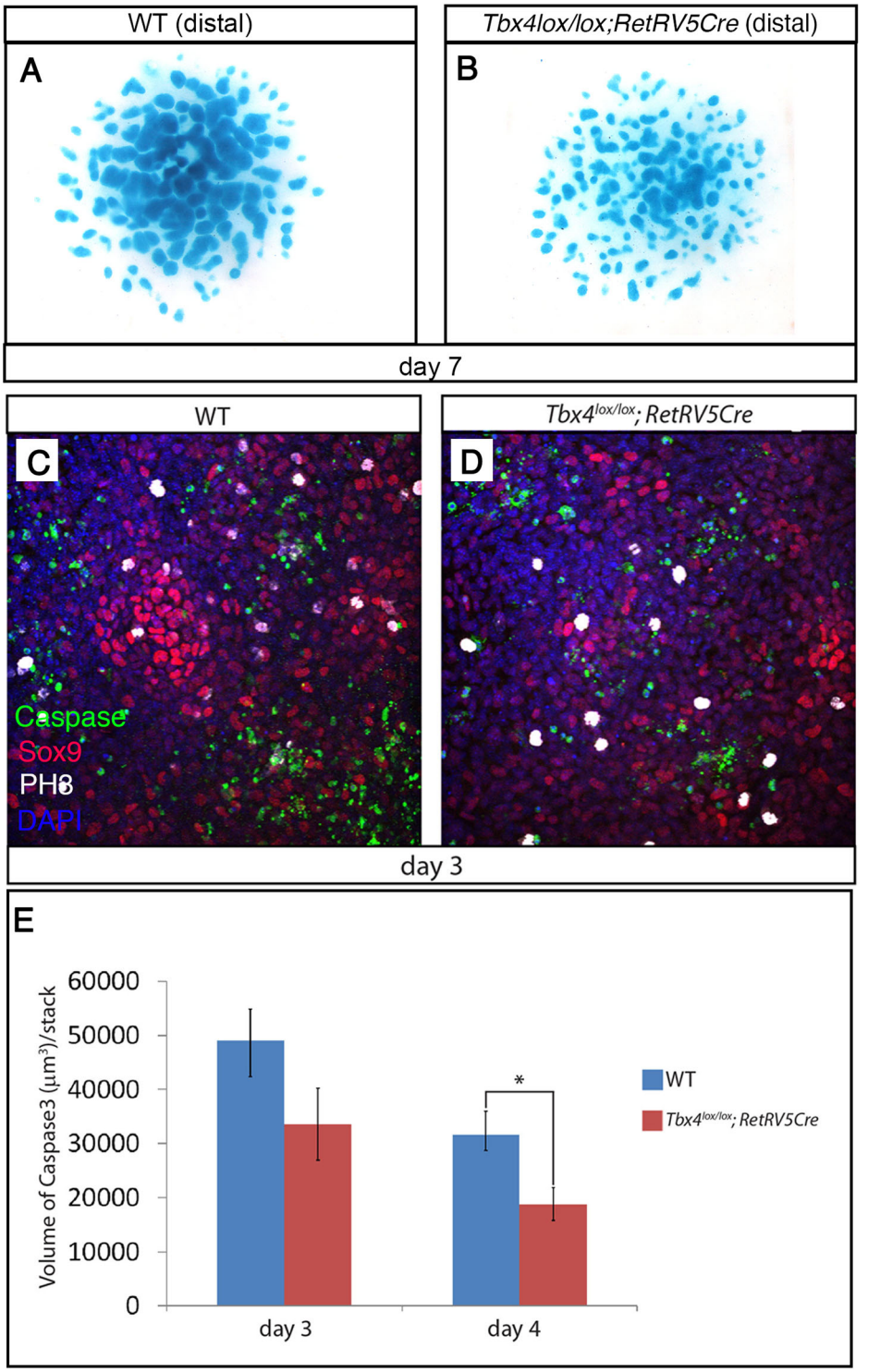

Fig. S5. Cell death is not responsible for the decreased number of chondroprogenitors detected over time. A,B Alcian Blue staining of cartilage nodule formation after 7 days of culture in micromass cultures established from distal cells of **(A)** Wild type hindlimbs (n=6), **(B)** *Tbx4lox/lox;RetRV5Cre* hindlimbs (n=6). **C,D** Extended focus confocal stacks of immunostained proximal micromass culture after 3 days culture. Anti-Caspase (green), anti-Sox9 (red), phospho-histone H3 (white) and nuclear staining (DAPI-blue) of control (C) and *Tbx4$^{lox/lox}$;RetRV5Cre* (D) proximal micromass. **(E)** Histogram showing mean ± s.e.m. volume in µm^3 of Caspase 3 staining measured in a stack at 20x magnification of control (blue) and *Tbx4$^{lox/lox}$;RetRV5Cre* (red) proximal micromass after 3 and 4 days of culture. No statistical difference is observed between the two conditions after Student *t*-test (P>0.05); n=5. Standard errors are shown.

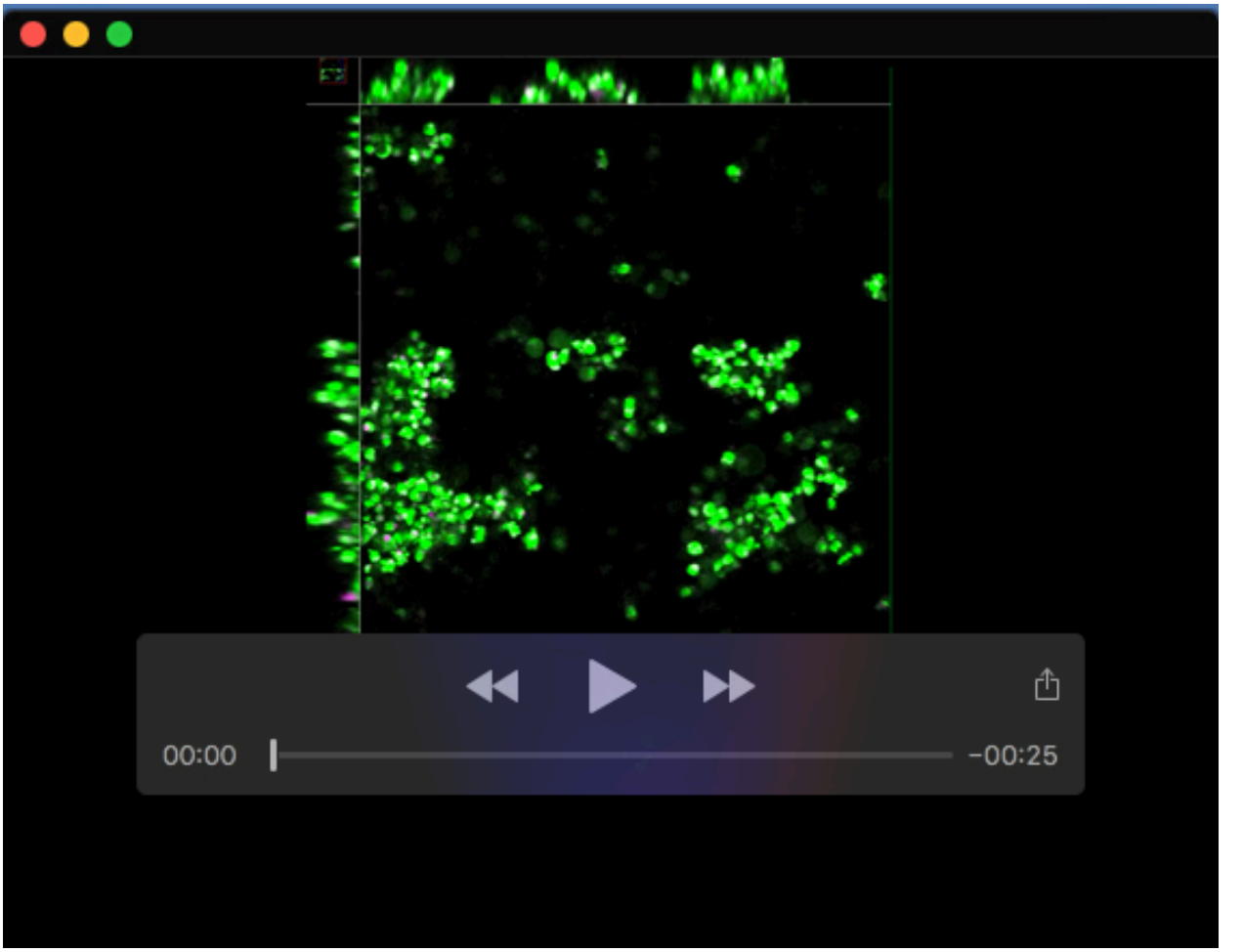

Movie 1. Time lapse movie of a control micromass culture stained with Cell Tracker dye. xyz views of Z-scan stacks imaged every 5 minutes during an 84hr culture. 20X magnification.

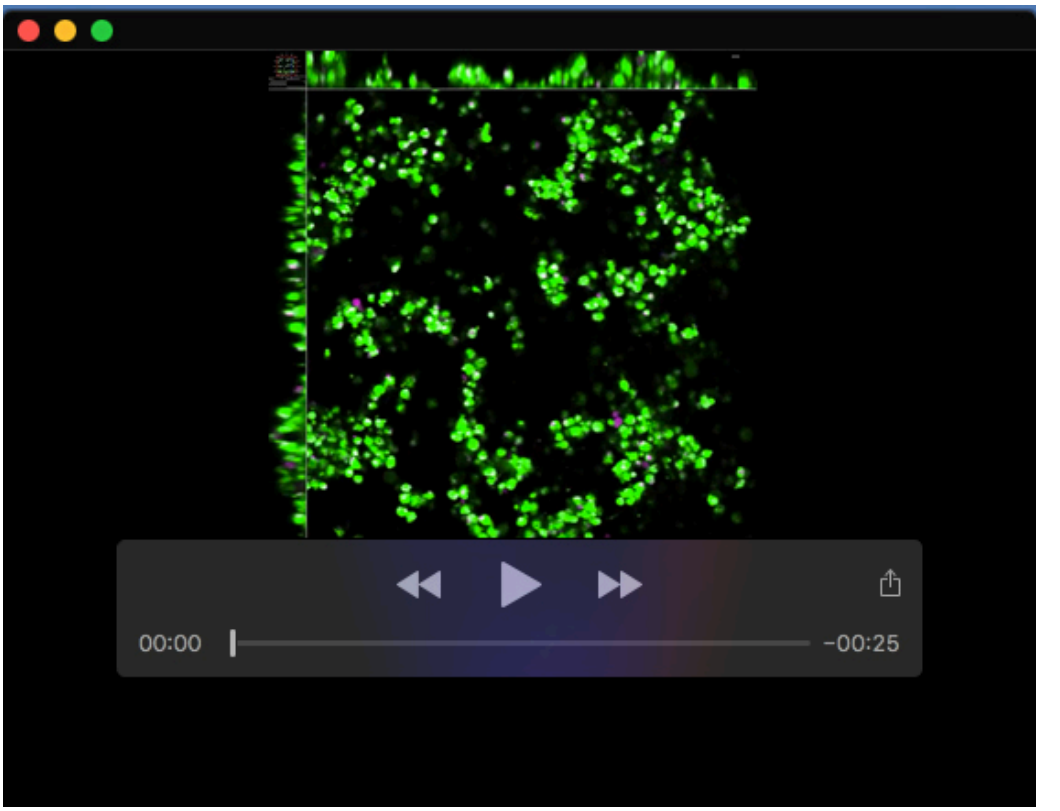

Movie 2. Time lapse movie of a *Tbx4*$^{lox/lox}$*;RetRV5Cre* micromass culture stained with Cell Tracker dye. xyz views of Z-scan stacks imaged every 5 minutes during an 84hr culture. 20X magnification.